FIGURE 1. **Binding analysis of IL-33 to ST2L-positive cells.** *A*, analysis of purified rIL-33 and rIL-1β. Purified proteins (100 ng) were separated on SDS-12.5% polyacrylamide gels, followed by silver staining (*panel a*) and Western blotting (*WB*) with anti-T7 tag (*αT7*), anti-mouse IL-33 (*αIL-33*), and anti-mouse IL-1β (*αIL-1β*) antibodies (*panel b*). *White* and *black arrowheads* indicate rIL-33 and rIL-1β, respectively. An *asterisk* indicates a cleaved product of rIL-1β. Protein size is indicated in kDa at the *left*. *B*, expression analysis of ST2L and IL-1RI in EL-4 cells. Stably transfected EL-4 cells were generated by introduction of an empty vector, an ST2L expression vector, or an IL-1RI expression vector (*EV, ST2L, or IL-1RI*). Stably transfected EL-4 cells (5 × 10⁵ cells) were stained with FITC-conjugated anti-mouse T1/ST2 antibody (*magenta line*), RPE-conjugated anti-mouse IL-1RI antibody (*green line*), or each isotype control antibody (*purple line*). The *gray-filled histogram* shows unstained cells. *C*, binding analysis of rIL-33 to EL-4 cells. Stably transfected EL-4 cells (5 × 10⁵ cells) were mixed with 100 ng (*blue line*) or 500 ng (*red line*) of rIL-33 for 1 h. Binding of rIL-33 was detected with biotinylated anti-T7 tag antibody and RPE-conjugated streptavidin. The *gray-filled histogram* shows unstained cells. *B* and *C*, the data of clone numbers 1-1-A-3 (EV/EL-4 cells), 1-2-G-12 (ST2L/EL-4 cells), and 3-2-A-8 (IL-1RI/EL-4 cells) are represented in each figure.

FLAG). Recombinant soluble ST2, expressed in HEK293T cells and secreted into the culture supernatant, was affinity-purified. The purity was confirmed by silver staining (Fig. 2*A*). SDS-PAGE analysis showed that purified recombinant soluble ST2 was detected as a single broad band of 55–65 kDa because of *N*-linked glycosylation. After deglycosylation with *N*-glycosidase F, the molecular mass shifted to 37 kDa, corresponding to an unmodified form. We tested whether soluble ST2 directly interacted with IL-33 *in vitro* (Fig. 2*B*). ST2-V5 was mixed with either rIL-33 or rIL-1β, and protein complexes were immunoprecipitated with anti-T7 tag antibody-conjugated agarose and then eluted from agarose. The eluates were analyzed by Western blotting using anti-V5 and anti-T7 tag antibodies. Analysis

of input was performed using the anti-His antibody because both recombinant proteins were His-tagged. These experiments clearly revealed that ST2-V5 specifically bound to rIL-33 but not to rIL-1β (Fig. 2*B*, compare *lanes 3–5*).

To further study the interaction between soluble ST2 and IL-33, we analyzed the binding of rIL-33 to ST2L/EL-4 cells or rIL-1β to IL-1RI/EL-4 cells in the presence of ST2-V5 (Fig. 2*C*). Stably transfected EL-4 cells were either left untreated or treated with ST2-V5 and then added with either rIL-33 or rIL-1β. ST2-V5 inhibited the binding of rIL-33 to ST2L/EL-4 cells (Fig. 2*C*, *upper panel*). In contrast, rIL-1β binding activity for IL-1RI/EL-4 cells was not affected in the presence of ST2-V5 (Fig. 2*C*, *lower panel*). Next, we examined whether the additive order of soluble ST2 influences the binding activity of IL-33 (Fig. 2*D*). ST2-V5 was added to ST2L/EL-4 cells before, after, or at the same time as the addition of rIL-33. When rIL-33 was added prior to ST2-V5, the binding of IL-33 was hardly influenced by the treatment with ST2-V5 (Fig. 2*D*, compare *panels c* and *d*). On the other hand, the binding of IL-33 was inhibited by the treatment with ST2-V5 at the same time or before the addition of rIL-33 (Fig. 2*D*, compare *panels c, e*, and *f*). In addition, the binding of ST2-V5 to ST2L/EL-4 cells was not observed regardless of the binding of IL-33 in this system. These results indicate that soluble ST2 specifically binds to free IL-33 and inhibits the binding activity of IL-33 for ST2L and that the ST2/IL-33 complex cannot bind to ST2L-positive cells.

Suppression of IL-33-induced NF-κB Activation by Soluble ST2—To study the activation of NF-κB by IL-33 signaling, we examined the DNA binding activity of NF-κB by EMSA and the degradation of IκBα by Western blotting (Fig. 3*A* and supplemental Fig. S1). Nuclear and cytoplasmic extracts were prepared from rIL-33- or rIL-1β-stimulated EL-4 cells. EMSA clearly showed that intracellular responses in the IL-33 and IL-1β signalings were consistent with the expression of ST2L and IL-1RI, respectively. Stimulation with rIL-33 specifically induced the DNA binding activity of NF-κB (Fig. 3*A, panel a, lane 6*) and the degradation of IκBα (Fig. 3*A, panel b, lane 5*) in ST2L-EL-4 cells. On the other hand, stimulation with rIL-1β
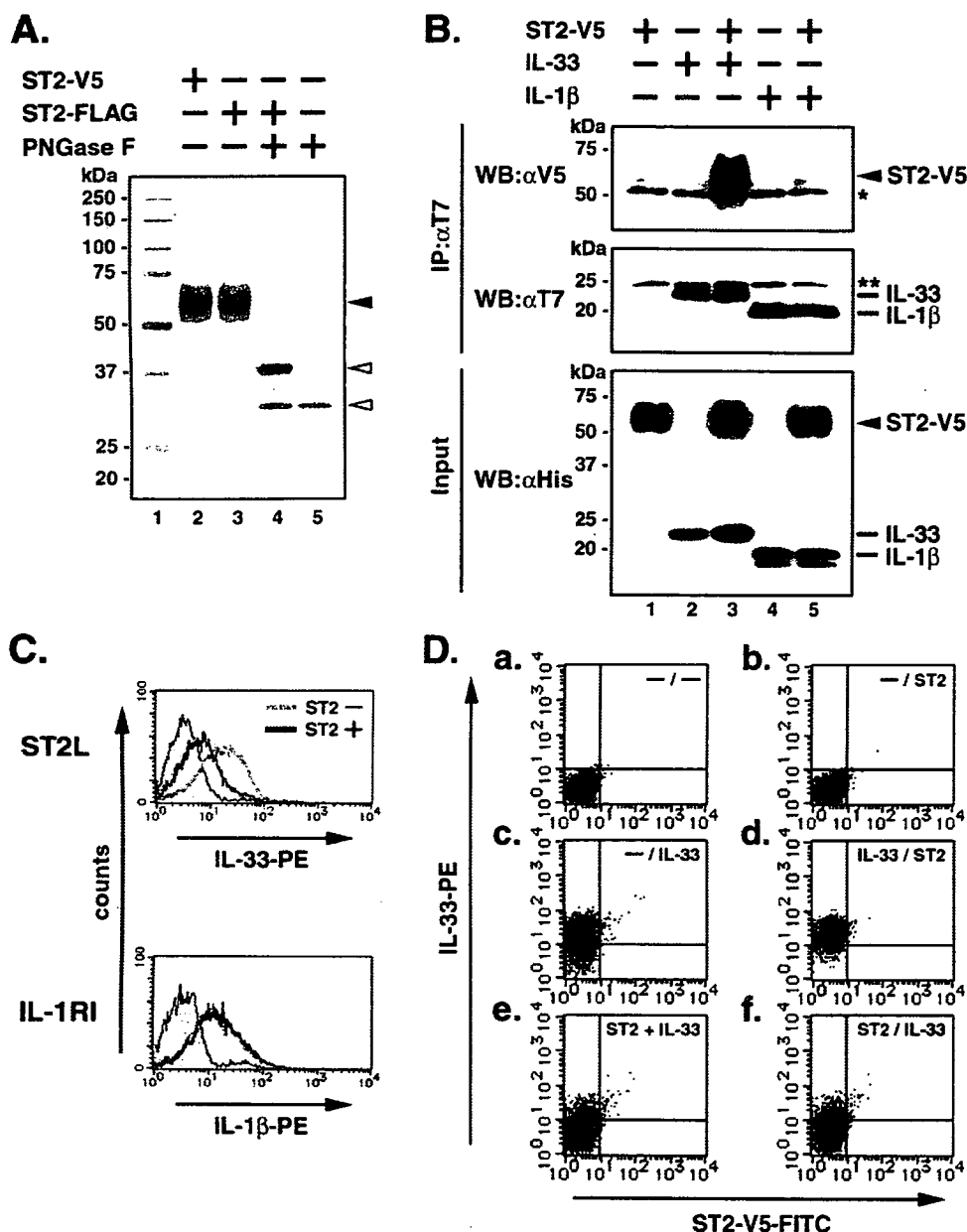
FIGURE 2. **Binding analysis of soluble ST2 to IL-33.** A, analysis of purified recombinant soluble ST2. Purified ST2-V5 and ST2-FLAG (100 ng) were left untreated or treated with N-glycosidase F. The proteins were separated on SDS-10% polyacrylamide gel, followed by silver staining. Glycosylated and deglycosylated proteins are indicated by black and gray arrowheads, respectively. N-Glycosidase F (PNGase F) is indicated by a white arrowhead. B, analysis of interaction between ST2-V5 and rIL-33, or rIL-1β. ST2-V5 (500 ng) was mixed with rIL-33 or rIL-1β (2 μg) in RIPA buffer. The protein complexes were immunoprecipitated with anti-T7 tag antibody-conjugated agarose (IP: αT7). The proteins were eluted with 0.1 M citric acid (pH 2.2) and neutralized with 2 M Tris (pH 10.4), followed by Western blotting (WB) with anti-V5 (αV5) and anti-T7 tag (αT7) antibodies. Input was analyzed by Western blotting with anti-His antibody (αHis) using 1/20 volumes of reaction mixture. Single and double asterisks indicate heavy and light chains of immunoglobulin, respectively. A and B, protein size is indicated in kDa at the left. C, effect of ST2-V5 on binding activity of rIL-33 or rIL-1β. Stably transfected EL-4 cells (5 × 10⁵ cells) were either left untreated or treated with ST2-V5 (1 μg) for 1 h, and then rIL-33 or rIL-1β (100 ng) was admixed for 1 h. Binding of rIL-33 or rIL-1β was detected with biotinylated anti-T7 tag antibody and RPE-conjugated streptavidin. Upper panel, binding of rIL-33 to ST2L/EL-4 cells (clone, 1-2-G-12). Lower panel, binding of rIL-1β to IL-1RI/EL-4 cells (clone, 3-2-A-8). Blue- and orange-lined histograms represent cells untreated or treated with ST2-V5, respectively. The gray-filled histogram shows unstained cells. D, effect of difference of ST2-V5-additive order on IL-33 binding activity. Binding of ST2-V5 was detected with FITC-conjugated anti-V5 antibody. The additive order of proteins was as follows: panel a, no addition (−/ −); panel b, ST2-V5 for 1 h alone (−/ST2); panel c, rIL-33 for 1 h alone (−/IL-33); panel d, rIL-33 for 1 h prior to ST2-V5 for another 1 h (IL-33/ST2); panel e, ST2-V5 and rIL-33 at the same time for 1 h (ST2 + IL-33); panel f, ST2-V5 for 1 h prior to rIL-33 for another 1 h (ST2/IL-33).

induced the activation of NF-κB (Fig. 3A, panel a, lanes 4, 7, and 10) and the degradation of IκBα (Fig. 3A, panel b, lanes 3, 6, and 9) in all cell lines, using constitutively expressed IL-1RI. Next,

we investigated components of activated NF-κB using specific antibodies against NF-κB. Supershift assay showed that the p50 and p65 subunits were contained in the IL-33-induced DNA/NF-κB complex (Fig. 3B, lanes 3 and 5), as well as in the IL-1β-induced DNA/NF-κB complex (Fig. 3B, lanes 8 and 10).

To further investigate the effect of soluble ST2 on IL-33 signaling, we examined the DNA binding activity of NF-κB and the degradation of IκBα in the presence of soluble ST2 (Fig. 3C and supplemental Fig. S2). Stably transfected EL-4 cells were either left untreated or treated with ST2-V5 and then were left unstimulated or stimulated with rIL-33 or rIL-1β. In IL-33-stimulated ST2L/EL-4 cells, the DNA/NF-κB complex was gradually decreased as the concentration of ST2-V5 increased (Fig. 3C, panel a, lanes 5–7). In contrast, pretreatment with ST2-V5 led to the repression of IκBα degradation (Fig. 3C, panel b, lanes 4–6). On the other hand, ST2-V5 did not affect the NF-κB activation and IκBα degradation in the IL-1β signaling (Fig. 3C, panel a, lanes 11–13, and panel b, lanes 10–12). In addition, we examined NF-κB-dependent luciferase activity in IL-33- or IL-1β-stimulated EL-4 cells (Fig. 3D). Stimulation with IL-33 effectively induced NF-κB-dependent luciferase activity in ST2L/EL-4 cells. The IL-33-induced luciferase activity also slightly increased in IL-1RI/EL-4 cells coincident with low expression levels of ST2L. Furthermore, pretreatment with ST2-V5 reduced the IL-33-induced luciferase activities in both cell lines. On the other hand, IL-1β-induced luciferase activities in both cell lines were not affected by the addition of ST2-V5. These results demonstrate that soluble ST2 specifically suppresses the activation of NF-κB by IL-33 signaling via ST2L.

Expression of Soluble ST2 and ST2L in a Murine Model of Asthma—Previous studies have shown that expressions of soluble ST2 and ST2L increased in asthma. To investigate the expressions of soluble ST2 and ST2L
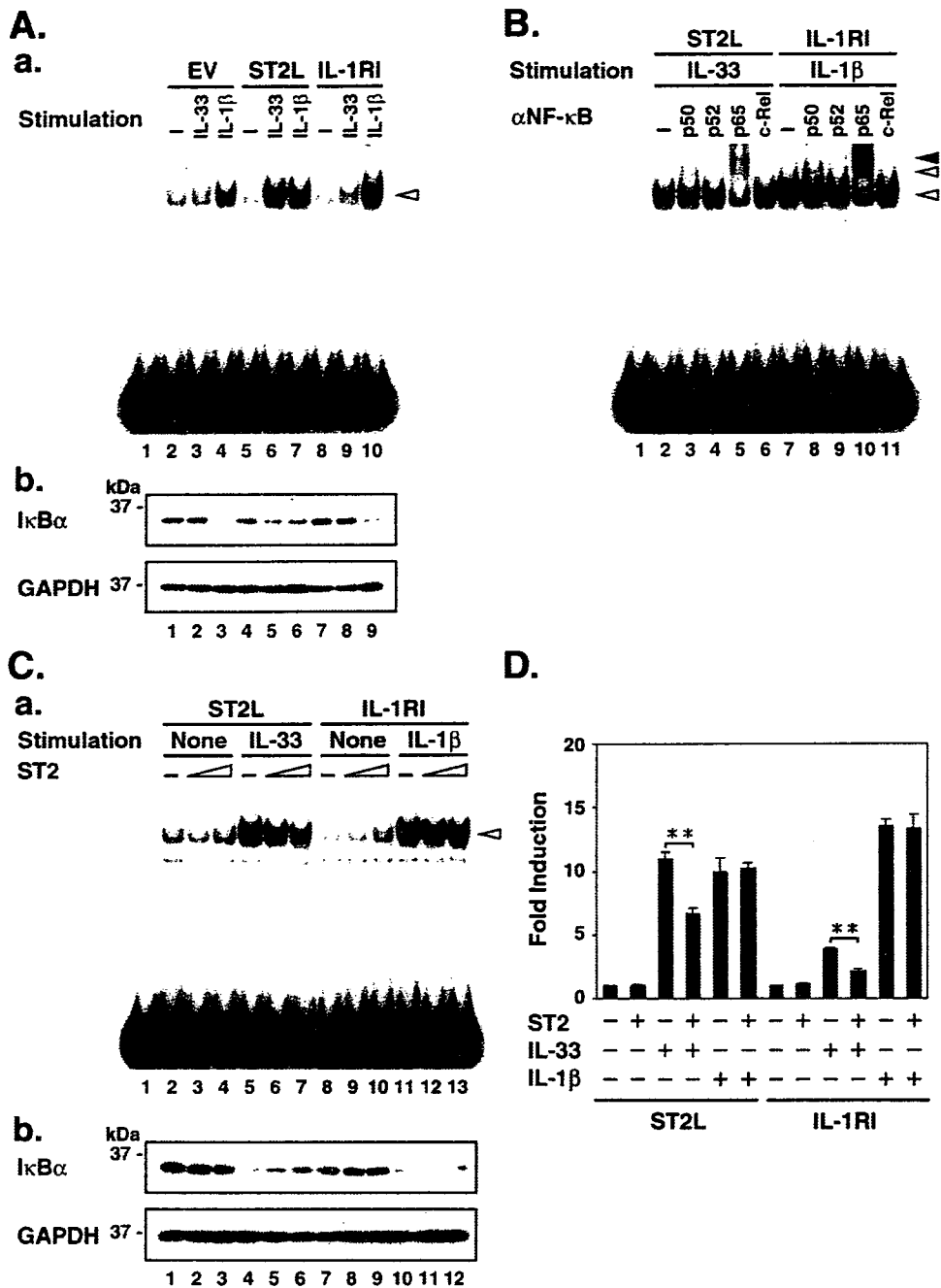
A.

a.

b.

B.

C.

a.

b.

D.

FIGURE 3. **Suppression of IL-33-induced NF-κB activation by soluble ST2.** *A,* analysis of intracellular responses in the IL-33 and IL-1β signalings. Stably transfected EL-4 cells (2 × 10^7 cells) were either left unstimulated or stimulated with rIL-33 or rIL-1β (10 ng/ml) for 30 min, followed by preparation of cytoplasmic and nuclear extracts. *Panel a,* EMSA using nuclear extracts with a ^{32}P-labeled oligonucleotide probe containing an NF-κB-binding site. The DNA-protein complexes were separated on a 4% nondenaturing polyacrylamide gel. *Panel b,* detection of IκBα and glyceraldehyde-3-phosphate dehydrogenase (*GAPDH*) in cytoplasmic extracts. Cytoplasmic extracts were separated on SDS-12.5% polyacrylamide gels, followed by Western blotting with anti-IκBα and anti-glyceraldehyde-3-phosphate dehydrogenase antibodies. *B,* supershift assay using anti-NF-κB antibodies. Nuclear extracts were kept on ice for 1 h without antibody (*lanes 2* and *7*) or with a series of anti-NF-κB antibodies (*lanes 3-6* and *8-11*), and then the ^{32}P-labeled oligonucleotide probe was admixed. The mixture was kept at 30 °C for 30 min and then subjected to EMSA. *C,* suppression of DNA binding activity of NF-κB by the addition of ST2-V5. Stably transfected EL-4 cells were either left untreated or treated with ST2-V5 (10 and 100 ng) for 3 h and then left unstimulated or stimulated with rIL-33 or rIL-1β for 30 min. After stimulation, cytoplasmic and nuclear extracts were prepared. *Panel a,* DNA binding activity of NF-κB was analyzed by EMSA. *Panel b,* degradation of IκBα was analyzed by Western blotting. *Lanes 1* of *A* (*panel a*), *B,* and *C* (*panel a*) contained the ^{32}P-labeled oligonucleotide probe alone. The DNA/NF-κB and supershifted complexes are indicated by *white, gray* (supershifted by αp50), and *black* (supershifted by αp65) *arrowheads,* respectively. *D,* transcriptional activity of rIL-33-or rIL-1β-induced NF-κB. Stably transfected EL-4 cells (1 × 10^7 cells) were transiently transfected with pNF-κB-Luc (40 μg) and pRL-TK (4 μg). The transfected cells were either left untreated or treated with ST2-V5 (500 ng/ml) for 3 h and then either left unstimulated or stimulated with rIL-33 or rIL-1β (10 ng/ml) for 24 h. The cells were harvested and subjected to luciferase assay. Firefly luciferase activity was normalized with *Renilla* luciferase activity, and the luciferase activity of the untreated and unstimulated cells was given a reference value of 1. The data are shown as the means ± S.E. from four independent experiments. **, $p < 0.01$, IL-33 alone *versus* ST2 plus IL-33). The data of clone numbers 1-1-A-3 (EV/EL-4 cells), 1-2-G-12 (ST2L/EL-4 cells), and 3-2-A-8 (IL-1RI/EL-4 cells) are represented in each panel.
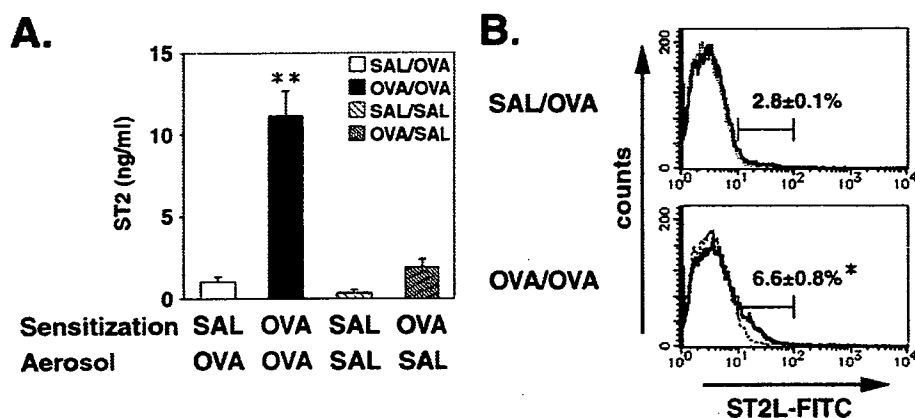
A.

B.

FIGURE 4. **Expression of soluble ST2 and ST2L in a murine model of asthma.** *A*, level of soluble ST2 in sera after aeroallergen challenge. The mice were sensitized with saline and challenged with OVA (*SAL/OVA*), sensitized and challenged with OVA (*OVA/OVA*), sensitized and challenged with saline (*SAL/SAL*), or sensitized with OVA and challenged with saline (*OVA/SAL*). The sera were obtained at 24 h after the last aeroallergen challenge. The concentration of soluble ST2 was measured by sandwich ELISA. The data are shown as the means ± S.E. (*n* = 10 mice/group; **, *p* < 0.01, OVA/OVA *versus* either SAL/OVA, SAL/SAL, or OVA/SAL). *B*, expression analysis of ST2L in splenocytes. Splenocytes were prepared from SAL/OVA and OVA/OVA mice at 24 h after the last OVA challenge. Splenocytes (1 × 10⁶ cells) were stained with FITC-conjugated anti-mouse T1/ST2 antibody (*solid line*) and then analyzed by flow cytometry. The *thin-lined histogram* shows unstained cells. Percentages of ST2L-positive splenocytes are shown as the means ± S.E. (*n* = 8 mice in SAL/OVA, *n* = 9 mice in OVA/OVA; *, *p* < 0.05, OVA/OVA *versus* SAL/OVA).

proteins *in vivo*, we utilized a murine model of asthma caused by OVA. BALB/c mice were sensitized with saline (SAL) or OVA and then challenged with an aerosol of SAL or OVA. Twenty-four hours after the last aeroallergen challenge, the concentration of soluble ST2 in sera was measured by sandwich ELISA, and the expression of ST2L in splenocytes was detected by flow cytometry. The level of soluble ST2 was predominantly elevated in OVA-sensitized and -challenged (OVA/OVA) mice (Fig. 4*A*). In contrast, the production of soluble ST2 in other groups was low and showed no significant difference. However, soluble ST2 was below the detectable level in bronchoalveolar lavage fluids of any groups in our sandwich ELISA system (data not shown). Moreover, the expression of ST2L in splenocytes was apparently induced in OVA/OVA mice. On the other hand, the expression of ST2L in SAL/OVA mice was as low as that in untreated mice (Fig. 4*B* and data not shown). These results indicate that the expressions of soluble ST2 and ST2L were specifically induced in asthmatic mice by the combination of sensitization and challenge with OVA.

In addition, we also examined the protein expression of IL-33 in asthmatic mice. So far, a detection system such as ELISA for secreted murine IL-33 has not been developed. Therefore, we tried to detect IL-33 protein by Western blotting using commercially available anti-mouse IL-33 antibody. Cellular extracts were prepared from the thymus of asthmatic mice because the expression of IL-33 mRNA was highly induced in the thymus (Fig. 5*A*). However, we could detect neither the precursor nor the mature IL-33 protein in this experiment.

Expression of ST2, ST2L, and IL-33 mRNAs after the OVA Challenge—To investigate the expressions of the ST2 and IL-33 genes in various tissues of OVA/OVA mice, we performed a reverse transcription-PCR analysis (Fig. 5). Expression of the ST2 gene was induced in the thymus, lung, lymph node, spleen, and ovary after the last OVA challenge. However, the expression in the brain, heart, liver, kidney, and skeletal muscle was

low or absent, as was the case for the testis (Fig. 5*A* and data not shown). Although the expression of the ST2 gene in the stomach was detected, the level of expression was not altered before and after the OVA challenge (data not shown). Interestingly, biphasic expression of the ST2 gene was observed in the thymus, lung, lymph node, and spleen. The expression of the ST2 gene was increased at 3 h, dropped at 6 h, and then increased again until 12 h or 24 h (Fig. 5). In addition, the expression profile was different in female and male mice. Expression of the ST2 gene was gradually induced in the ovary after the OVA challenge, but not in the testis. In the expression of the IL-33 gene, pronounced biphasic expression was observed in the thymus and lung (Fig. 5). IL-33 mRNA was expressed in the lymph node, ovary, and testis; however, the expression was hardly observed in the spleen. These results indicate that the expression of the ST2 gene is induced in immunological response-associated tissues after the OVA challenge and that the expression of the IL-33 gene is also induced in several tissues of asthmatic mice.

Suppression of the Production of Th2 Cytokines from IL-33-stimulated Splenocytes—A previous study showed that IL-33 induces the production of Th2 cytokines (9). To study the effects of soluble ST2 on the biological activity of IL-33, we analyzed the production of Th2 cytokines from splenocytes of asthmatic mice. We first examined whether rIL-33 binds to splenocytes using flow cytometry (Fig. 6*A*). Splenocytes were prepared from SAL/OVA and OVA/OVA mice at 24 h after the last OVA challenge. Recombinant IL-33 apparently bound to ST2L-positive splenocytes prepared from OVA/OVA mice. Next, we analyzed the production of Th1 and Th2 cytokines. Fig. 6*B* shows a scheme for the stimulation of splenocytes. The splenocytes were stimulated with OVA for activation of lymphocytes. The OVA-stimulated splenocytes were either untreated or treated with ST2-FLAG for 3 h. Subsequently, the splenocytes were left unstimulated or stimulated with rIL-33 for 48 h, followed by harvest of culture supernatants. Stimulation with rIL-33 specifically induced the productions of IL-4, IL-5, and IL-13 from splenocytes of OVA/OVA mice, whereas the production of these cytokines was reduced by pretreatment with ST2-FLAG (Fig. 6*C*). On the other hand, the production of IFN-γ was increased according to the reduction of Th2 cytokine production in splenocytes of OVA/OVA mice. Although the production of IFN-γ from splenocytes of SAL/OVA mice was also induced by the addition of IL-33 alone or ST2-FLAG plus IL-33, the reasons are presently unclear. Where the splenocytes of OVA/OVA mice were unstimulated with OVA, IL-33-induced production of Th2 cytokines was low (data not shown). These results suggest that IL-33 induces the production of Th2
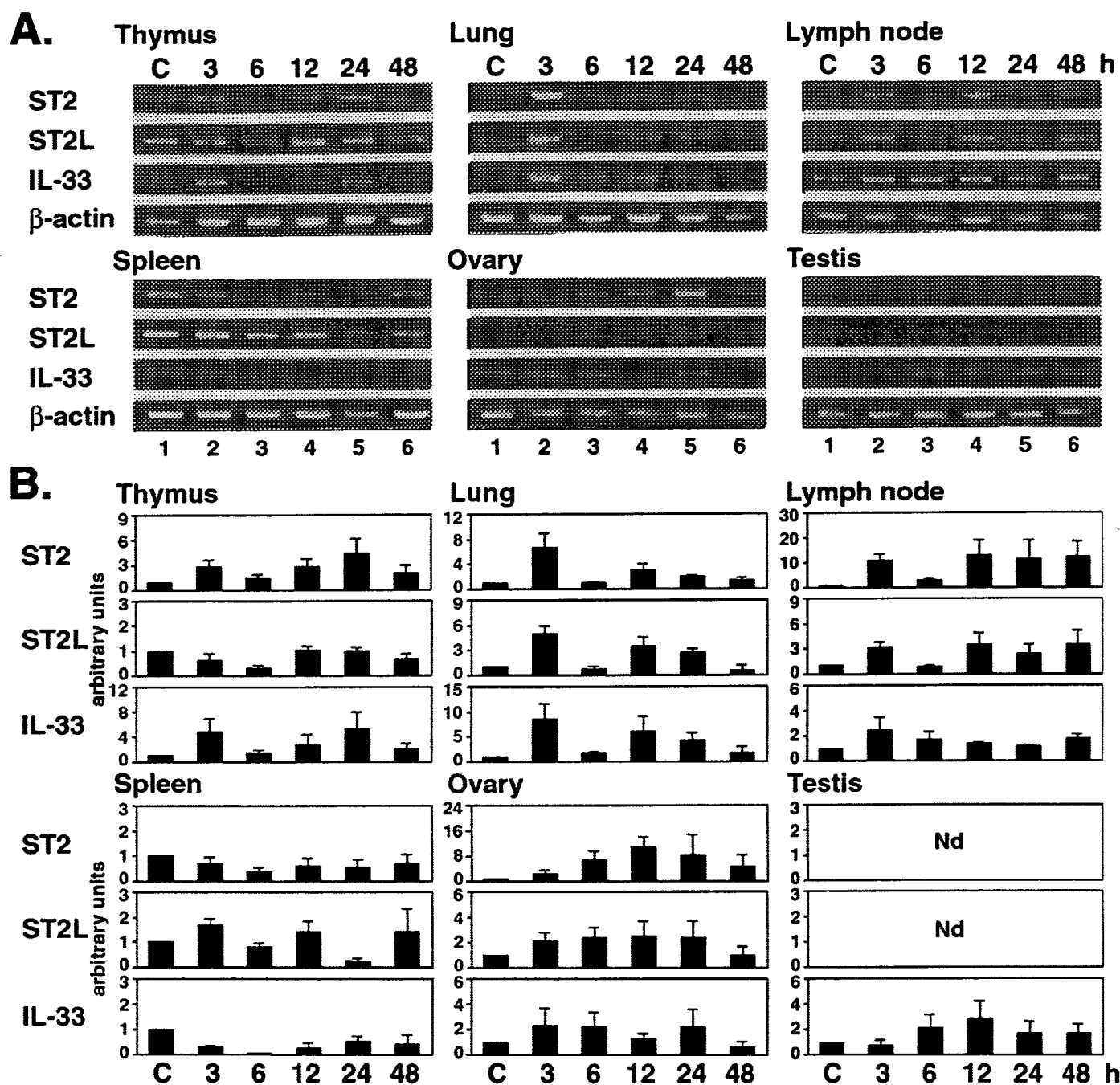
A.

B.

FIGURE 5. **Expression of ST2, ST2L, and IL-33 mRNAs after the last OVA challenge.** *A*, reverse transcription-PCR analysis of expression of ST2, ST2L, and IL-33 mRNAs in tissues of asthmatic mice. DNase I-treated total RNAs were prepared from tissues of untreated mice (*control*; lanes *C*) and OVA/OVA mice at the indicated time shown above each lane (*3–48 h*) after the last OVA challenge and then were subjected to reverse transcription-PCR analysis. *β*-Actin was detected as an internal control. PCR products were separated on 2% agarose gels. The data show one of three independent experiments. *B*, kinetic analysis of expression of ST2, ST2L, and IL-33 mRNAs. Densitometric analysis was performed using the public domain NIH Image program. Expression of ST2, ST2L, and IL-33 mRNAs was normalized with that of *β*-actin mRNA, and expression of control mice was given a reference value of 1. The data are shown as arbitrary units (means ± S.E.) from three independent experiments. *Nd*, no data for low level of gene expression.

cytokines from activated splenocytes via ST2L. Taken together, soluble ST2 suppresses the IL-33-induced production of Th2 cytokines.

DISCUSSION

This study has examined the regulation of IL-33 signaling by the soluble secreted form of the ST2 gene products (soluble ST2). We found that soluble ST2 has antagonistic effects on IL-33 signaling in allergic airway inflammation.

IL-33 is a member of the IL-1 cytokine family; the intracellular pathway of IL-33 signaling is similar to that of IL-1 signaling (9). We have studied IL-33 signaling using EL-4 cells stably expressing ST2L or IL-1RI (Figs. 1 and 3). IL-33 specifically bound to ST2L/EL-4 cells, but not to IL-1RI/EL-4 cells. The binding of IL-33 to ST2L induced the degradation of IκBα and subsequent activation of DNA binding activity of NF-κB. IL-33-induced DNA/NF-κB complex contained the p50 and p65 subunits. Furthermore, we found that soluble ST2 also bound to

A.

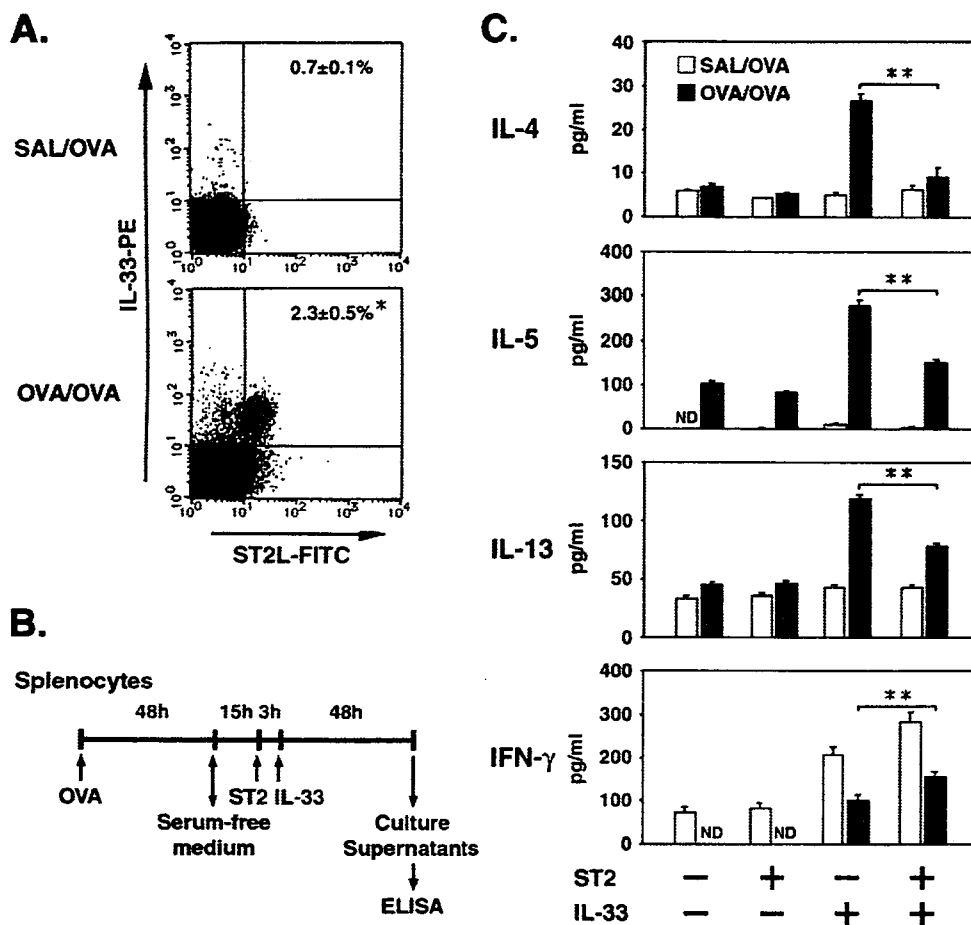**B.**

Splenocytes

C.

FIGURE 6. **Suppression of Th2 cytokine production from IL-33-stimulated splenocytes of asthmatic mice.** *A*, binding analysis of rIL-33 to splenocytes by flow cytometry. Splenocytes were prepared from SAL/OVA and OVA/OVA mice at 24 h after the last OVA challenge. The splenocytes (1×10^6 cells) were mixed with rIL-33 (1 μg) for 1 h. The splenocytes were stained with biotinylated anti-T7 tag antibody, RPE-conjugated streptavidin, and FITC-conjugated anti-mouse T1/ST2 antibody. Percentages of IL-33-bound ST2L-positive splenocytes are shown as the means $\pm$ S.E. ($n = 8$ mice in SAL/OVA, $n = 9$ mice in OVA/OVA; *, $p < 0.05$, OVA/OVA *versus* SAL/OVA). *B*, schematic diagram for stimulation of splenocytes. The splenocytes were prepared from SAL/OVA and OVA/OVA mice at 24 h after the last OVA challenge. Stimulation of splenocytes was performed as described under "Experimental Procedures." After the culture supernatants were harvested, the concentrations of IL-4, IL-5, IL-13, and IFN-γ were measured by ELISA. *C*, levels of Th1 and Th2 cytokines in culture supernatants. *White* and *black bars* indicate data obtained from splenocytes of SAL/OVA and OVA/OVA mice, respectively. The data are shown as the means $\pm$ S.E. ($n = 8$ mice in SAL/OVA, $n = 9$ mice in OVA/OVA; **, $p < 0.01$, IL-33 alone *versus* ST2 plus IL-33 in splenocytes of OVA/OVA mice). *ND*, not detected.

IL-33 and that pretreatment with soluble ST2 suppressed the IL-33-induced NF-κB activation in ST2L/EL-4 cells (Figs. 2 and 3). Thus, our results indicate that the binding activity of IL-33 for ST2L was inhibited by the formation of an ST2/IL-33 complex, leading to the suppression of IL-33 signaling.

Several studies have shown that soluble forms of cytokine receptors function as positive or negative regulators in the expression of cytokines and growth factors. The soluble form of IL-1 receptor type II (sIL-1RII), IL-4 receptor α-chain (sIL-4Rα), and IL-13 receptor α-chain 2 (sIL-13Rα2) have antagonistic effects on IL-1, IL-4, and IL-13 signalings, respectively (20–22). In contrast, the soluble IL-6 receptor α-chain (sIL-6Rα) has agonistic effects on IL-6 signaling and modulates the expression of chemokines (23, 24). Soluble forms of cytokine receptors are generated by several mechanisms including alternative splicing of pre-mRNA and proteolytic cleavage of receptors (25). In the case of the ST2 protein, soluble ST2 is generated by alternative splicing of pre-mRNA, and its amino acid

sequence is mostly consistent with that of the extracellular domain of ST2L (1, 3). Therefore, it was a reasonable result that soluble ST2 possessed binding activity for IL-33. Besides soluble ST2 and ST2L, ST2V in humans and ST2LV in chickens have been reported as variant forms of the ST2 gene products (26–28). These variants might also be related to the regulation of IL-33 signaling because of containing the extracellular domain.

In patients and model mice of allergic asthma, the level of soluble ST2 was elevated in sera (14, 15), and the number of CD4-positive T cells expressing ST2L was increased in the lung and lymph nodes (29). On the other hand, the expression of IL-33 in allergic asthma is not investigated yet. In this study, we demonstrated that the expression of IL-33 mRNA was induced in several tissues after the OVA challenge in a murine model of asthma (Fig. 5). In addition, IL-33 bound to ST2L-positive splenocytes of asthmatic mice and induced the productions of IL-4, IL-5, and IL-13 (Fig. 6). Although we could not clarify a level and a time course for protein expression of IL-33, these results suggest that IL-33 expresses and functions as a cytokine in allergic asthma. Furthermore, we showed a detailed expression profile of the ST2 gene in asthmatic mice. The ST2 gene was predominantly expressed in the thymus, lung, lymph nodes, and spleen (Fig. 5). The expression of the ST2 gene in these tissues was regulated by the distal promoter (data not shown), which functions in Th2 cell-mediated immunological responses (16, 30). The biphasic expression pattern of ST2 mRNA corresponds to the production pattern of soluble ST2 in sera after the OVA challenge (15), suggesting that these tissues might be sources of soluble ST2. In addition, the level of soluble ST2 in sera was dramatically elevated in comparison with that of ST2L on the cell surfaces of splenocytes after the OVA challenge (Fig. 4). This drastic increase of the soluble ST2 concentration may contribute to the suppression of IL-33 signaling *in vivo*. In fact, pretreatment with soluble ST2 was effective for the suppression of IL-4, IL-5, and IL-13 productions from IL-33-stimulated splenocytes in asthmatic mice (Fig. 6). This negative effect on Th2 cytokine production was consistent with the results of therapeutic experiments using a recombinant soluble ST2-Fc protein or a soluble ST2 expression vector (7, 15). Thus, our results strongly support the paradigm that soluble ST2 neg-

atively regulates the production of Th2 cytokines in allergic airway inflammation.

Serum levels of soluble ST2 have been found to be elevated in various diseases such as rheumatoid arthritis, systemic lupus erythematosus, and idiopathic pulmonary fibrosis (31, 32), as well as asthma. In addition, soluble ST2 suppresses the production of inflammatory cytokines by stimulation with lipopolysaccharides in murine macrophages and THP-1 cells, derived from human monocytic leukemia (18, 33). Therefore, soluble ST2 may participate in the regulation of inflammatory cytokines besides Th2 cytokines.

NF-κB is a key regulator in the IL-33 signaling pathway, although it remains unclear how NF-κB regulates the expression of the Th2 cytokine genes. Previous studies using animal models have provided evidence that NF-κB plays an essential role in Th2 cell-mediated immunological responses. The p50-deficient ($p50^{-/-}$) and c-Rel-deficient (c-Rel$^{-/-}$) mice do not develop allergic airway inflammation (34, 35). Furthermore, p50 is required for the expression of transcription factor GATA-3, which regulates the expression of Th2 cytokine genes (36). Transgenic mice expressing dominant negative GATA-3 exhibit the inhibition of allergic inflammation (37). Hereafter, analysis of the downstream regulation of NF-κB is required to advance understanding of IL-33 signaling. In addition, the processing mechanism of the IL-33 protein has not been elucidated *in vivo*. A recent study reported that pre-IL-33 also functioned as a transcriptional repressor in nucleus besides acting as a cytokine (38). Therefore, the regulation for secretion of native IL-33 protein should be studied for better understanding of the biological and pathological functions of IL-33.

In conclusion, we showed the biological function of soluble ST2 *in vitro* and *in vivo*. We demonstrated that soluble ST2 suppresses the activation of NF-κB and the production of Th2 cytokines in IL-33 signaling, suggesting that this suppression leads to attenuation of allergic inflammatory responses in asthma. Furthermore, our findings may serve to advance knowledge in relation to the biological functions of IL-33 and therapeutic effects of soluble ST2 in allergic airway inflammation.

REFERENCES

1. Tominaga, S. (1989) *FEBS Lett.* **258**, 301–304
2. Klemenz, R., Hoffmann, S., and Werenskiold, A. K. (1989) *Proc. Natl. Acad. Sci. U. S. A.* **86**, 5708–5712
3. Yanagisawa, K., Takagi, T., Tsukamoto, T., Tetsuka, T., and Tominaga, S. (1993) *FEBS Lett.* **318**, 83–87
4. Gächter, T., Werenskiold, A. K., and Klemenz, R. (1996) *J. Biol. Chem.* **271**, 124–129
5. Yanagisawa, K., Naito, Y., Kuroiwa, K., Arai, T., Furukawa, Y., Tomizuka, H., Miura, Y., Kasahara, T., Tetsuka, T., and Tominaga, S. (1997) *J. Biochem. (Tokyo)* **121**, 95–103
6. Xu, D., Chan, W. L., Leung, B. P., Huang, F., Wheeler, R., Piedrafita, D., Robinson, J. H., and Liew, F. Y. (1998) *J. Exp. Med.* **187**, 787–794
7. Löhning, M., Stroehmann, A., Coyle, A. J., Grogan, J. L., Lin, S., Gutierrez-Ramos, J. C., Levinson, D., Radbruch, A., and Kamradt, T. (1998) *Proc.*

Natl. Acad. Sci. U. S. A. **95**, 6930–6935
8. Lécart, S., Lecointe, N., Subramaniam, A., Alkan, S., Ni, D., Chen, R., Boulay, V., Pène, J., Kuroiwa, K., Tominaga, S., and Yssel, H. (2002) *Eur. J. Immunol.* **32**, 2979–2987
9. Schmitz, J., Owyang, A., Oldham, E., Song, Y., Murphy, E., McClanahan, T. K., Zurawski, G., Moshrefi, M., Qin, J., Li, X., Gorman, D. M., Bazan, J. F., and Kastelein, R. A. (2005) *Immunity* **23**, 479–490
10. Baekkevold, E. S., Roussigné, M., Yamanaka, T., Johansen, F. E., Jahnsen, F. L., Amalric, F., Brandtzaeg, P., Erard, M., Haraldsen, G., and Girard, J. P. (2003) *Am. J. Pathol.* **163**, 69–79
11. Dinarello, C. A. (1996) *Blood* **87**, 2095–2147
12. Tsutsui, H., Matsui, K., Okamura, H., and Nakanishi, K. (2000) *Immunol. Rev.* **174**, 192–209
13. Townsend, M. J., Fallon, P. G., Matthews, D. J., Jolin, H. E., and McKenzie, A. N. (2000) *J. Exp. Med.* **191**, 1069–1076
14. Oshikawa, K., Kuroiwa, K., Tago, K., Iwahana, H., Yanagisawa, K., Ohno, S., Tominaga, S., and Sugiyama, Y. (2001) *Am. J. Respir. Crit. Care Med.* **164**, 277–281
15. Oshikawa, K., Yanagisawa, K., Tominaga, S., and Sugiyama, Y. (2002) *Clin. Exp. Allergy* **32**, 1520–1526
16. Hayakawa, M., Yanagisawa, K., Aoki, S., Hayakawa, H., Takezako, N., and Tominaga, S. (2005) *Biochim. Biophys. Acta* **1728**, 53–64
17. Takagi, T., Yanagisawa, K., Tsukamoto, T., Tetsuka, T., Nagata, S., and Tominaga, S. (1993) *Biochim. Biophys. Acta* **1178**, 194–200
18. Takezako, N., Hayakawa, M., Hayakawa, H., Aoki, S., Yanagisawa, K., Endo, H., and Tominaga, S. (2006) *Biochem. Biophys. Res. Commun.* **341**, 425–432
19. Tago, K., Funakoshi, M., Mano, H., Yanagisawa, K., Hayakawa, M., Kuroiwa, K., Iwahana, H., Kasahara, T., and Tominaga, S. (2001) *Eur. J. Biochem.* **268**, 6526–6533
20. Giri, J. G., Wells, J., Dower, S. K., McCall, C. E., Guzman, R. N., Slack, J., Bird, T. A., Shanebeck, K., Grabstein, K. H., Sims, J. E., and Alderson, M. R. (1994) *J. Immunol.* **153**, 5802–5809
21. Sato, T. A., Widmer, M. B., Finkelman, F. D., Madani, H., Jacobs, C. A., Grabstein, K. H., and Maliszewski, C. R. (1993) *J. Immunol.* **150**, 2717–2723
22. Zhang, J. G., Hilton, D. J., Willson, T. A., McFarlane, C., Roberts, B. A., Moritz, R. L., Simpson, R. J., Alexander, W. S., Metcalf, D., and Nicola, N. A. (1997) *J. Biol. Chem.* **272**, 9474–9480
23. Peters, M., Jacobs, S., Ehlers, M., Vollmer, P., Müllberg, J., Wolf, E., Brem, G., Meyer zum Buschenfelde, K. H., and Rose-John, S. (1996) *J. Exp. Med.* **183**, 1399–1406
24. Hurst, S. M., Wilkinson, T. S., McLoughlin, R. M., Jones, S., Horiuchi, S., Yamamoto, N., Rose-John, S., Fuller, G. M., Topley, N., and Jones, S. A. (2001) *Immunity* **14**, 705–714
25. Levine, S. J. (2004) *J. Immunol.* **173**, 5343–5348
26. Tominaga, S., Kuroiwa, K., Tago, K., Iwahana, H., Yanagisawa, K., and Komatsu, N. (1999) *Biochem. Biophys. Res. Commun.* **264**, 14–18
27. Tago, K., Noda, T., Hayakawa, M., Iwahana, H., Yanagisawa, K., Yashiro, T., and Tominaga, S. (2001) *Biochem. Biophys. Res. Commun.* **285**, 1377–1383
28. Iwahana, H., Hayakawa, M., Kuroiwa, K., Tago, K., Yanagisawa, K., Noji, S., and Tominaga, S. (2004) *Biochim. Biophys. Acta* **1681**, 1–14
29. Gajewska, B. U., Swirski, F. K., Alvarez, D., Ritz, S. A., Goncharova, S., Cundall, M., Snider, D. P., Coyle, A. J., Gutierrez-Ramos, J. C., Stämpfli, M. R., and Jordana, M. (2001) *Am. J. Respir. Cell Mol. Biol.* **25**, 326–334
30. Shimizu, M., Matsuda, A., Yanagisawa, K., Hirota, T., Akahoshi, M., Inomata, N., Ebe, K., Tanaka, K., Sugiura, H., Nakashima, K., Tamari, M., Takahashi, N., Obara, K., Enomoto, T., Okayama, Y., Gao, P. S., Huang, S. K., Tominaga, S., Ikezawa, Z., and Shirakawa, T. (2005) *Hum. Mol. Genet.* **14**, 2919–2927
31. Kuroiwa, K., Arai, T., Okazaki, H., Minota, S., and Tominaga, S. (2001) *Biochem. Biophys. Res. Commun.* **284**, 1104–1108
32. Tajima, S., Oshikawa, K., Tominaga, S., and Sugiyama, Y. (2003) *Chest* **124**, 1206–1214
33. Sweet, M. J., Leung, B. P., Kang, D., Sogaard, M., Schulz, K., Trajkovic, V., Campbell, C. C., Xu, D., and Liew, F. Y. (2001) *J. Immunol.* **166**, 6633–6639

34. Yang, L., Cohn, L., Zhang, D. H., Homer, R., Ray, A., and Ray, P. (1998) *J. Exp. Med.* 188, 1739–1750
35. Donovan, C. E., Mark, D. A., He, H. Z., Liou, H. C., Kobzik, L., Wang, Y., De Sanctis, G. T., Perkins, D. L., and Finn, P. W. (1999) *J. Immunol.* 163, 6827–6833
36. Das, J., Chen, C. H., Yang, L., Cohn, L., Ray, P., and Ray, A. (2001) *Nat. Immunol.* 2, 45–50
37. Zhang, D. H., Yang, L., Cohn, L., Parkyn, L., Homer, R., Ray, P., and Ray, A. (1999) *Immunity* 11, 473–482
38. Carriere, V., Roussel, L., Ortega, N., Lacorre, D. A., Americh, L., Aguilar, L., Bouche, G., and Girard, J. P. (2007) *Proc. Natl. Acad. Sci. U. S. A.* 104, 282–287

Adenoassociated Virus–Mediated Prostacyclin Synthase Expression Prevents Pulmonary Arterial Hypertension in Rats

Takayuki Ito, Takashi Okada, Jun Mimuro, Hiroshi Miyashita, Ryosuke Uchibori, Masashi Urabe, Hiroaki Mizukami, Akihiro Kume, Masafumi Takahashi, Uichi Ikeda, Yoichi Sakata, Kazuyuki Shimada, Keiya Ozawa

Abstract—Prostacyclin synthase (PGIS) is the final committed enzyme in the metabolic pathway of prostacyclin production. The therapeutic option of intravenous prostacyclin infusion in patients with pulmonary arterial hypertension is limited by the short half-life of the drug and life-threatening catheter-related complications. To develop a better delivery system for prostacyclin, we examined the feasibility of intramuscular injection of an adenoassociated virus (AAV) vector expressing PGIS for preventing monocrotaline-induced pulmonary arterial hypertension in rats. We developed an AAV serotype 1–based vector carrying a human PGIS gene (AAV-PGIS). AAV-PGIS or the control AAV vector expressing enhanced green fluorescent protein was injected into the anterior tibial muscles of 3-week–old male Wistar rats; this was followed by the monocrotaline administration at 7 weeks. Eight weeks after injecting the vector, the plasma levels of 6-keto-prostaglandin $F_{1\alpha}$ increased in a vector dose-dependent manner. At this time point, the PGIS transduction (1×10^{10} genome copies per body) significantly decreased mean pulmonary arterial pressure (33.9 ± 2.4 versus 46.1 ± 3.0 mm Hg; $P < 0.05$), pulmonary vascular resistance (0.26 ± 0.03 versus 0.41 ± 0.03 mm Hg $\cdot$ mL^{-1} $\cdot$ min^{-1} $\cdot$ kg^{-1}; $P < 0.05$), and medial thickness of the peripheral pulmonary artery ($14.6 \pm 1.5\%$ versus $23.5 \pm 0.5\%$; $P < 0.01$) as compared with the controls. Furthermore, the PGIS-transduced rats demonstrated significantly improved survival rates as compared with the controls (100% versus 50%; $P < 0.05$) at 8 weeks postmonocrotaline administration. An intramuscular injection of AAV-PGIS prevents monocrotaline-pulmonary arterial hypertension in rats and provides a new therapeutic alternative for preventing pulmonary arterial hypertension in humans. (*Hypertension.* 2007;50:531-536.)

Key Words: hypertension ■ pulmonary ■ gene therapy ■ remodeling ■ prostacyclin synthase

Pulmonary arterial hypertension (PAH) is an intractable disease that leads to increased pulmonary arterial pressure, progressive right heart failure, and premature death; however, no satisfactory treatment has been established for PAH.[1] Although intravenous prostacyclin (PGI$_2$) therapy prolongs survival in patients with PAH, the use of this treatment option is limited by the short half-life of the drug, requirement for a continuous infusion system, and catheter-related complications.[1,2] PGI$_2$ synthase (PGIS) is the final committed enzyme in the metabolic pathway of PGI$_2$ production. PGIS gene transfer is a promising approach for the stable production of endogenous PGI$_2$.[3–6] However, previous strategies have several limitations both in the selection of delivery routes and in the efficiency of gene expression. For instance, intratracheal gene transfer may deteriorate respiratory function in critically ill subjects, and the intrahepatic

approach may cause peritonitis as a result of direct liver puncture. Although an intramuscular approach seems to be safer than the previous approaches, the conventional plasmid-based strategies achieved only transient gene expression and required repeated gene transfer to inhibit pathological remodeling of the pulmonary artery (PA).[6]

In this study, we used an adenoassociated virus (AAV) vector together with an intramuscular approach to obtain more efficient PGI$_2$ expression. AAV vectors permit efficient and sustained gene expression in nondividing skeletal muscle cells with minimal inflammatory and immune responses. We reported previously that a stable serum concentration of a secretory protein was achieved over a 1-year period by using a single intramuscular injection of several AAV vector (AAV2 and AAV5) serotypes in mice.[7] Currently, AAV1 is one of the most efficient serotypes for muscle transduction.[8,9]

Single subcutaneous injection of a pyrrolizidine alkaloid, namely, monocrotaline (MCT), produces severe PAH and PA remodeling in rats. We examined the effects of sustained PGIS expression in preventing PAH development and progression by means of this widely used model and an AAV1 vector.

Methods

Western Blot Analysis for PGIS Expression In Vitro

Human embryonic kidney 293 (HEK293) cells were incubated in 10-cm dishes containing DMEM and nutrient mixture F12 (Invitrogen) with 2% FCS in an atmosphere of 5% CO_2 in air at 37°C. The cells at 70% confluence were transfected with an AAV proviral plasmid encoding human PGIS (phPGIS, a kind gift from Dr Mimuro) or plasmid encoding enhanced green fluorescent protein (eGFP) by using a calcium phosphate method. The cells were harvested 72 hours after transfection, and cell lysates were prepared with a lysis buffer (10 mmol/L of Tris-HCl, 150 mmol/L of NaCl, and 1% NP40 [pH 7.6]) containing Complete Mini protease inhibitor (Roche Diagnostics). For Western blot analysis, 10 μg of the lysate was subjected to 10% SDS-PAGE and transferred to a nitrocellulose membrane. The membrane was blocked and incubated with a 1:500 dilution of rabbit anti-human PGIS polyclonal antibody (a gift from Dr Mimuro) and a 1:5000 dilution of peroxidase-linked anti-rabbit IgG antibody (Amersham Pharmacia Biotech), and immunoreactive bands were visualized using an enhanced chemiluminescence Western blotting kit (Amersham).

AAV-PGIS Production and PGI_2 Expression

We developed a recombinant AAV1-based vector containing the human PGIS or eGFP gene controlled by a modified chicken β-actin promoter with a cytomegalovirus immediate-early enhancer (AAV-PGIS or AAV-eGFP) to obtain efficient transgene expression in skeletal muscle cells. The AAV vectors were prepared according to the previously described 3-plasmid transfection adenovirus-free protocol with minor modifications for enabling the use of an active gassing system.[10,11] In brief, 60% confluent HEK293 cells that were incubated in a large culture vessel with active air circulation were cotransfected with phPGIS, AAV-1 chimeric helper plasmid (p1RepCap), and adenoviral helper plasmid pAdeno (Avigen Inc). The crude viral lysate was purified with 2 rounds of cesium chloride 2-tier centrifugation.[12] The titer of the viral stock was determined against plasmid standards by real-time PCR with primers 5'-CCCGCGAGGTTGTGGTGGAC-3' and 5'-ATGGGCGGATGCG-GTAGC-3'; subsequently, the stock was dissolved in a buffer (50 mmol/L of HEPES [pH 7.4] and 0.15 mol/L of NaCl [HN buffer]) before infection. The HEK293 cells cultured in 6-well plates containing DMEM and nutrient mixture F12 with 5% FCS were infected with AAV-PGIS at 1×10^4 genome copies per cell to evaluate PGI_2 expression in vitro, and the supernatant was harvested after 72 hours. Concentrations of 6-keto-prostaglandin $F_{1\alpha}$ (6-keto-$PGF_{1\alpha}$) in plasma or culture media were determined by enzyme immunoassay (R&D Systems) according to the manufacturer's instructions. The minimum detectable dose of the assay was <1.4 pg/mL. Interassay and intra-assay precision of the kit was <10%.

Animal Models

All of the animal experiments were approved by the Jichi Medical University ethics committee and were performed in accordance with the National Institutes of Health Guide for the Care and Use of Laboratory Animals. To evaluate the efficiency of gene expression in vivo, AAV-eGFP (200 μL; 1×10^{11} gene copies per body) or AAV-PGIS (200 μL; 1×10^{10} to 1×10^{11} gene copies per body) was injected into the bilateral anterior tibial muscles (n=3 each) of 3-week-old male Wistar rats (Clea Japan Inc) weighing 45 to 55 g. For hemodynamics and histological analyses, the rats were divided into 4 groups: sham rats that were administered the HN buffer (group

1, negative control [NC] group; n=4); MCT-PAH rats administered the HN buffer (group 2, MCT group; n=6); MCT rats administered AAV-eGFP (group 3, MCT+eGFP group; n=6); and MCT rats administered AAV-PGIS (group 4, MCT+PGIS group; n=10). After the anesthesia with spontaneous inhalation of 1% isoflurane, the rats in groups 3 and 4 were intramuscularly injected with AAV-eGFP or AAV-PGIS (1×10^{10} gene copies per body), whereas those in groups 1 and 2 were injected with the HN buffer (200 μL). MCT (Wako Pure Chemicals) was dissolved in 0.1 N HCl, and the pH was adjusted to 7.4 with 1.0 N NaOH. After the anesthesia with spontaneous inhalation of 1% isoflurane, all of the rats except for those in the NC group were injected subcutaneously with MCT (40 mg/kg) 4 weeks after the injecting the vector. Blood samples were collected from the tail vein on ethylenediamine tetraacetic acid tubes, and the concentrations of the leukocytes, platelets, hematocrit, alanine aminotransferase, and creatinine were determined by standard procedures.

Hemodynamics Analysis

Four weeks after the MCT injection, the rats were anesthetized with spontaneous inhalation of 1% isoflurane, and a tracheotomy was performed. Then, they were mechanically ventilated with 1% isoflurane (tidal volume, 10 mL/kg; respiratory rate, 30 breaths per minute) through a tracheostomy. After the thoracic cavity was opened using a midsternal approach, 2F high-fidelity manometer-tipped catheters (SPC-320; Millar Instruments Inc) were inserted directly into the right or left ventricle, and an ultrasonic flow probe (flow probe 2.5S176; Transonic Systems Inc) was placed on the ascending root of the aorta. The heart rate, mean pulmonary arterial pressure (mPAP), aortic systolic arterial pressure, left ventricular end-diastolic pressure (LVEDP), and mean aortic flow indicating the cardiac output (CO) were measured. Cardiac indices (CI) and pulmonary vascular resistance (PVR) were calculated using the following formula: CI (mL · min^{-1} · kg^{-1})=CO/body weight, PVR (mm Hg · mL^{-1} · min^{-1} · kg^{-1})=(mPAP−LVEDP)/CI.

Ventricular Weight Measurement and Morphometric Analysis of the PA

After the hemodynamic analysis, the rats were killed with an overdose (5%) of isoflurane through a tracheostomy. Their lungs were perfused with 5 mL of saline followed by 10 mL of cold 4% paraformaldehyde. Each ventricle and the lungs were then excised, dissected free, and weighed. The weight ratio of the right ventricle to the left ventricle plus septum [RV/(LV+S)] was calculated as an index of right ventricular hypertrophy (RVH). The lung tissues were fixed overnight at 4°C in 4% paraformaldehyde and frozen in Tissue-Tek OCT compound (Sakura Finetechnical Co) at −20°C. Hematoxylin and eosin staining was performed on 7-μm–thick sections that were subsequently examined using light microscopy. A morphometric analysis was performed on a PA having an external diameter of 25 to 50 μm or 51 to 100 μm. The medial wall thickness was calculated using the following formula: medial thickness (%)=medial wall thickness/external diameter×100.[13] For the quantitative analysis, 30 vessels of each rat were measured and averaged randomly by the 2 external observers.

Survival Analysis

The 3-week-old Wistar rats were divided into 3 groups (MCT, MCT+eGFP, and MCT+PGIS; n=8 each). After the anesthesia with spontaneous inhalation of 1% isoflurane, the rats in the MCT+eGFP or MCT+PGIS group were intramuscularly injected with AAV-eGFP or AAV-PGIS at 1×10^{10} genome copies per body, respectively. Under the same anesthetic condition, all of the rats were injected subcutaneously with MCT (40 mg/kg) at 4 weeks after injecting the vector. The survival rate was estimated from the date of the MCT administration until death or after 8 weeks of the injection. Survival curves were analyzed using the Kaplan-Meier method and compared by log-rank tests.
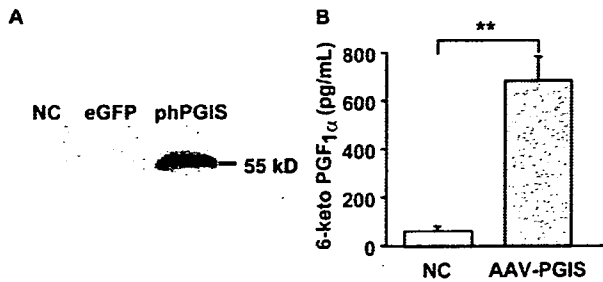
Figure 1. Expression of PGIS and PGI$_2$ in vitro. A, Western blot analysis of PGIS expression in HEK293 cells after plasmid transfection. The cells were harvested 72 hours after transfection with phPGIS or eGFP. B, AAV vector-mediated PGI$_2$ expression in HEK293 cells. The PGI$_2$ levels were estimated by measuring the amount of 6-keto-PGF$_{1\alpha}$, a stable metabolite of PGI$_2$, in the culture supernatant by enzyme immunoassay 72 hours after infecting the cells (n=4 each) with AAV-PGIS (1×10^4 genome copies per cell). Data are presented as mean±SEM. $^{**}P<0.01$. NC indicates untreated negative control.

Statistical Analysis

The statistical analysis and correlations were performed using StatView (Abacus Concepts, Inc). Data are presented as mean±SEM. Differences in parameters were evaluated using ANOVA combined with Fisher's test. A value of $P<0.05$ was considered statistically significant.

Results

Expression of PGIS and PGI$_2$ In Vitro

Western blot analysis revealed that transfection of the HEK293 cells with phPGIS but not with a plasmid carrying the eGFP gene enhanced the production of the PGIS protein (Figure 1A). Infection of the cells with AAV-PGIS at 1×10^4 genome copies per cell significantly increased the concentration of 6-keto-PGF$_{1\alpha}$, a stable metabolite of PGI$_2$, in culture supernatants as compared with that without vector infection (Figure 1B).

AAV Vector-Mediated Systemic PGI$_2$ Expression in the Rats

Four weeks after the injection of AAV vectors (1×10^{10} genome copies per body), the PGIS-transduced rats began exhibiting significant increases in the plasma 6-keto-PGF$_{1\alpha}$ levels as compared with the control rats (Figure 2A). Eight weeks after the injection, the 6-keto-PGF$_{1\alpha}$ levels increased further in a vector dose-dependent manner in the treated rats (Figure 2B) as compared with the untreated controls (6.68±1.33 versus 1.62±0.30 ng/mL, 1×10^{11} versus 1×10^{10} genome copies per body, respectively; $P<0.05$; n=3 each). The vectors at 1×10^{10} genome copies per body were used for all of the subsequent experiments. In contrast, injection of 1×10^{11} genome copies per body of AAV-eGFP produced no significant change in the 6-keto-PGF$_{1\alpha}$ levels.

Effects of PGI$_2$ Expression on Hemodynamics and RVH

Four weeks after the MCT administration, the mPAP levels were significantly elevated in the treated rats as compared with the untreated controls (Figure 3A). Treatment with AAV-PGIS but not AAV-eGFP significantly inhibited this increase (Figure 3A). In addition, the expression of PGI$_2$
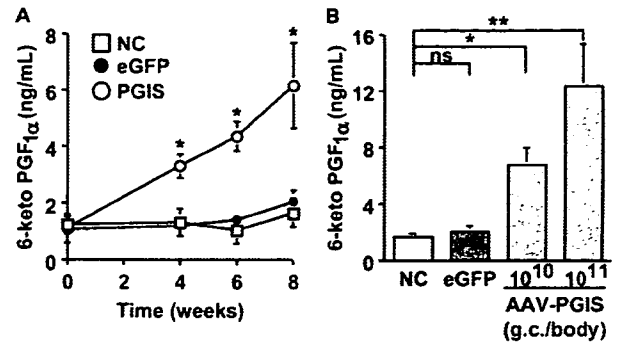

Figure 2. AAV vector-mediated systemic expression of PGI$_2$ in vivo. The concentration of plasma 6-keto-PGF$_{1\alpha}$ was determined by enzyme immunoassay after a single injection of AAV-PGIS into the anterior tibial muscle of 3-week-old male Wistar rats. A, Time course of plasma 6-keto-PGF$_{1\alpha}$ levels after injection of AAV-PGIS at 1×10^{10} genome copies per body. B, Vector dose dependency of plasma 6-keto-PGF$_{1\alpha}$ levels 8 weeks after the injection. The rats injected with AAV-eGFP (1×10^{11} genome copies per body) were used as controls. Data are presented as mean±SEM (n=3 animals per group). ns indicates not statistically significant; NC, untreated negative control. $^*P<0.05$ vs NC; $^{**}P<0.01$.

significantly mitigated an increase in PVR and a decrease in CI that were induced by MCT (Figure 3B and 3C, respectively); however, it produced no significant changes in the heart rate and aortic systolic arterial pressure (Table). PGI$_2$ expression also had a beneficial effect on RVH. Treatment with AAV-PGIS but not AAV-eGFP significantly inhibited the MCT-induced increase in RV/(LV+S) (Figure 3D).

Effects on Medial Hypertrophy of the PA

Medial hypertrophy is a hallmark of pathological vascular remodeling in PAH. Four weeks after the MCT injection, the
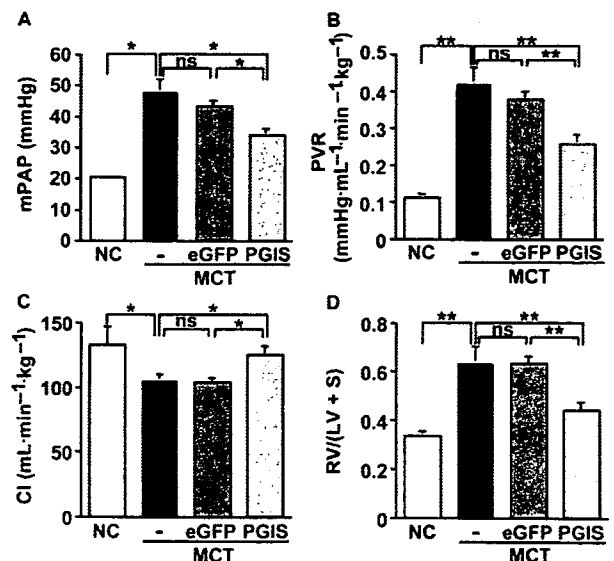

Figure 3. Effects of PGI$_2$ on hemodynamics and RVH. A quantitative analysis was performed using MCT-induced PAH rats 8 weeks after injecting the vector. A, mPAP (mm Hg); B, PVR (mm Hg · mL^{-1} · min^{-1} · kg^{-1}); C, CI (mL · min^{-1} · kg^{-1}). D, Weight ratio of the right ventricle to the left ventricle plus septum [RV/(LV+S)] presented as an index of RVH. Data are presented as means±SEM (n=4 to 10 animals per group). $^*P<0.05$; $^{**}P<0.01$. ns indicates not statistically significant; NC, untreated negative control.

Physiological and Laboratory Data of the MCT-Induced PAH Rats

Factor	NC	MCT	MCT+eGFP	MCT+PGIS	P
No. of rats	4	6	6	10	...
Heart rate, per minute	294.0±10.6	281.2±14.7	268.0±9.0	274.8±8.7	NS
ASAP, mm Hg	99.5±1.6	97.3±2.0	96.3±2.4	94.7±4.4	NS
Body weight, g	358.5±11.5	328.3±7.2	328.0±11.4	342.5±9.8	NS
Leukocyte, per mL	6725±372	7917±723	8800±849	8030±852	NS
Hematocrit, %	48.2±0.7	48.9±1.9	51.0±3.0	47.8±1.8	NS
Platelet, ×10⁴/mm³	88.3±8.7	79.2±8.8	80.4±3.6	84.6±6.3	NS
ALT, IU/L	37.8±2.5	49.5±8.4	52.5±6.8	44.1±4.3	NS
Cr, mg/dL	0.52±0.04	0.59±0.05	0.48±0.03	0.53±0.04	NS

Data are presented as means±SEM (n=4 to 10 animals per group). ASAP indicates aortic systolic arterial pressure; ALT, serum alanine aminotransferase; Cr, serum creatinine; NS, not statistically significant.

medial thickness of the PA was greater in the MCT-administered rats than in the untreated controls (Figure 4A). Treatment with AAV-PGIS but not AAV-eGFP prevented the MCT-induced increase in the percentage of medial thickness significantly (Figure 4B, 25 to 50 μm; Figure 4C, 51 to 100 μm in external diameter).

Effects on the Survival of the MCT-PAH Rats and Their Organ Dysfunctions

The PGIS-transduced rats exhibited significantly improved survival rates as compared with the eGFP-transduced rats (Figure 5). The MCT administration produced a slight but not significant decrease in the body weight of the rats, and PGIS gene transfer prevented this decrease. Although the MCT group showed only a slight but not significant increase in the leukocyte count and serum alanine aminotransferase levels as compared with the NC group, the AAV-PGIS treatment caused no additional change in these parameters (Table).

Discussion

The present study demonstrates that sustained PGI₂ expression by a single intramuscular injection of AAV-PGIS pre-vents the development of MCT-PAH in rats. PGI₂ expression not only increased the cardiac output significantly but also prevented the progression of PVR, RVH, and medial hypertrophy of the PA that was induced by the MCT administration. The PGIS-transduced rats also exhibited significantly improved survival rates as compared with the controls. Furthermore, the PGIS expression observed in this study caused no additional adverse effects on hematologic data and serum indicators of hepatorenal function (alanine aminotransferase and creatinine levels) in the MCT-PAH rats.

The expression of PGI₂ and PGIS decreased in the remodeled PAs of the idiopathic PAH patients.[14,15] Impaired PGI₂ synthesis resulting from a decrease in PGIS expression may be implicated in the pathogenesis of PAH. In fact, continuous intravenous infusion of exogenous PGI₂ markedly lowers PVR and improves survival in PAH patients. However, this system requires lifelong infusion with a central venous catheter because of the short biological half-life of PGI₂. Furthermore, because this system is associated with life-threatening complications (eg, shock and sepsis) that may result in poor survival and quality of life of patients, stable
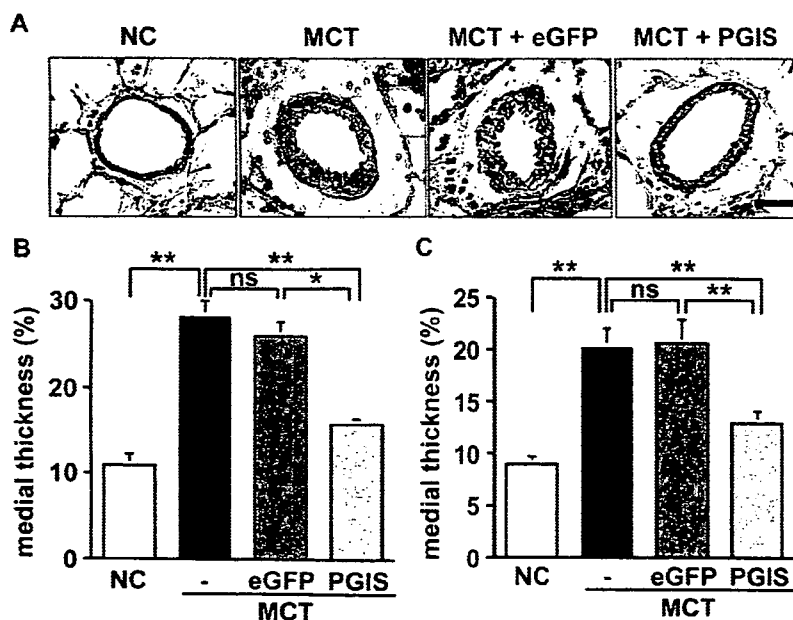

Figure 4. Effects of PGI₂ on medial hypertrophy of the peripheral PA. A, Representative cross-sections of the peripheral PA 4 weeks after the MCT administration (hematoxylin and eosin staining, original magnification, ×1000; scale bar=20 μm). B and C, Quantitative analysis of percentage of medial thickness (B, 25 to 50 μm; C, 51 to 100 μm in external diameter). Data are presented as means±SEM (n=4 to 10 animals per group). *P<0.05, **P<0.01. ns indicates not statistically significant; NC, untreated negative control.
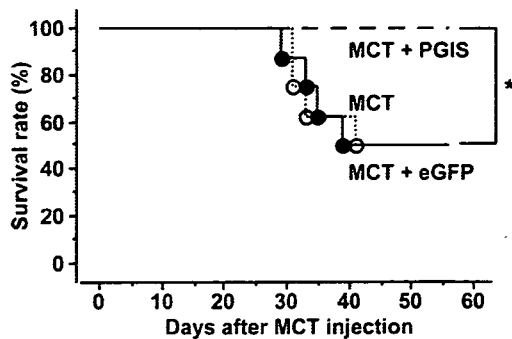
Figure 5. The survival rate of MCT-induced PAH rats. The rats were administered with MCT (40 mg/kg) 4 weeks after the injection of HN buffer (MCT group), AAV-eGFP (MCT+eGFP group), or AAV-PGIS (MCT+PGIS group). The rats were intramuscularly injected with the vectors at 1×10^{10} genome copies per body. The Kaplan-Meier method demonstrated a significant improvement in the survival rate of the rats in the MCT+PGIS group as compared with those in either the MCT or MCT+eGFP group at 8 weeks post-MCT administration. n=8 animals per group; *$P<0.05$ vs MCT or eGFP groups.

production of endogenous PGI_2 would be more desirable. Consistent with previous gene therapy studies, our strategy presented high levels of endogenous PGI_2 expression. In addition, this strategy caused no systemic hypotension and hyperdynamic heart failure, which are the major adverse effects arising from uncontrolled blood levels during intravenous delivery of exogenous PGI_2.[3,4,6]

In this study, we used an AAV serotype 1 vector because it is effective not only in efficient muscle transduction but also in long-term secretion of therapeutic proteins into the systemic circulation. The cDNA for human PGIS shares a high identity with its rat counterpart.[16] In fact, the administration of a plasmid or hemagglutinating virus of the Japan-liposome vector encoding human PGIS successfully ameliorated MCT-PAH. However, the use of these vectors requires repeated administration for achieving sustained gene expression.[3-5] In contrast, the AAV vector used in this study achieved PGIS expression with a single intramuscular injection, and this expression was sustained for 1 year.[7]

Furthermore, gene transfer was believed to be safer when performed via an intramuscular approach as opposed to the intratracheal or intrahepatic approaches.[6] Currently, researchers are using adenoviral gene transfer in most clinical trials because of its high efficiency for gene expression. However, the potential toxic effects of adenoviruses, such as strong immunogenicity, are well known. In contrast, the intramuscular administration of AAV vectors is a promising strategy for delivering therapeutic proteins safely and efficiently, and their use has been examined in clinical trials for hemophilia.[17]

Although PGI_2 is known to be a short-acting vasodilator, recent studies have shown its antiremodeling effects when used in high doses. The administration of PGI_2 analogues cicaprost and iloprost in high concentrations ($>10^{-7}$ mol/L) inhibits mitogen-induced proliferation of rat primary PA smooth muscle cells in a cAMP-dependent manner.[18] Interestingly, another PGI_2 analogue, treprostinil, also inhibits the proliferation of human and mouse primary lung fibroblasts through the activation of a peroxisome proliferator-activated

receptor-β/δ when used in equivalent doses.[19] These observations suggest that high levels of PGI_2 may attenuate PA remodeling in vivo through antiproliferative effects. Consistent with previous studies, we demonstrated that high levels of endogenous PGI_2 successfully attenuated medial hypertrophy of the PA.[3,4,6] To discover new drug targets, the roles of peroxisome proliferator-activated receptors and high-level PGI_2 in PAH therapy should be determined, because peroxisome proliferator-activated receptors are associated with many inflammatory and proliferative disorders, including PAH.[2,20]

Finally, we will discuss the clinical implications and limitations of this study. Consistent with previous studies, maximum gene expression was noted 6 to 8 weeks after the intramuscular injection of AAV vectors. AAV-PGIS was injected 4 weeks before MCT administration for the transgene expression to reach plateau levels when MCT-PAH was fully developed (3 to 4 weeks after the injection). Our results are completely based on a preventive protocol, which may be rare in a clinical setting. However, PGI_2 is an established therapeutic molecule, and the advantage of early initiation of PGI_2 therapy for improving survival in patients with idiopathic PAH has been demonstrated in a large clinical trial.[21] These observations convinced us to propose the possible preemptive use of AAV-PGIS as a strategy to maintain basal levels of PGI_2 in patients with mild symptoms of PAH or in those identified as high-risk subjects who have not experienced PAH. As an alternative, the combined use of AAV-PGIS and an initial infusion of intravenous PGI_2 might be promising; the intravenous infusion should be tapered when sufficient levels of PGI_2 are attained. To evaluate the efficacy of AAV-PGIS in a therapeutic protocol (ie, vector injection after the development of PAH), use of a chronic hypoxic PAH model or newly developed self-complementary AAV vectors that can express transgenes earlier than the conventional vectors should be considered.[22]

Perspectives

The present study has demonstrated that the single intramuscular injection of AAV-PGIS achieved a sustained expression of PGI_2. This expression retarded the progression of MCT-PAH in rats without causing significant adverse effects. Thus, this strategy provides a new therapeutic alternative for PAH patients. However, the system in this study lacks the ability to regulate excessive transgene expression. Therefore, regulatory mechanisms to ensure adequate gene expression should be established to facilitate successful translation of this strategy in a clinical setting.

Acknowledgment

Sources of Funding

Sports, Science and Technology of Japan; and the Research Award to Jichi Medical School Graduate Student.

References

1. Humbert M, Sitbon O, Simonneau G. Treatment of pulmonary arterial hypertension. *N Engl J Med.* 2004;351:1425–1436.
2. Ito T, Ozawa K, Shimada K. Current drug targets and future therapy of pulmonary arterial hypertension. *Curr Med Chem.* 2007;14:719–733.
3. Nagaya N, Yokoyama C, Kyotani S, Shimonishi M, Morishita R, Uematsu M, Nishikimi T, Nakanishi N, Ogihara T, Yamagishi M, Miyatake K, Kaneda Y, Tanabe T. Gene transfer of human prostacyclin synthase ameliorates monocrotaline-induced pulmonary hypertension in rats. *Circulation.* 2000;102:2005–2010.
4. Suhara H, Sawa Y, Fukushima N, Kagisaki K, Yokoyama C, Tanabe T, Ohtake S, Matsuda H. Gene transfer of human prostacyclin synthase into the liver is effective for the treatment of pulmonary hypertension in rats. *J Thorac Cardiovasc Surg.* 2002;123:855–861.
5. Ono M, Sawa Y, Mizuno S, Fukushima N, Ichikawa H, Bessho K, Nakamura T, Matsuda H. Hepatocyte growth factor suppresses vascular medial hyperplasia and matrix accumulation in advanced pulmonary hypertension of rats. *Circulation.* 2004;110:2896–2902.
6. Tahara N, Kai H, Niiyama H, Mori T, Sugi Y, Takayama N, Yasukawa H, Numaguchi Y, Matsui H, Okumura K, Imaizumi T. Repeated gene transfer of naked prostacyclin synthase plasmid into skeletal muscles attenuates monocrotaline-induced pulmonary hypertension and prolongs survival in rats. *Hum Gene Ther.* 2004;15:1270–1278.
7. Yoshioka T, Okada T, Maeda Y, Ikeda U, Shimpo M, Nomoto T, Takeuchi K, Nonaka-Sarukawa M, Ito T, Takahashi M, Matsushita T, Mizukami H, Hanazono Y, Kume A, Ookawara S, Kawano M, Ishibashi S, Shimada K, Ozawa K. Adeno-associated virus vector-mediated interleukin-10 gene transfer inhibits atherosclerosis in apolipoprotein E-deficient mice. *Gene Ther.* 2004;11:1772–1779.
8. Chen S, Kapturczak MH, Wasserfall C, Glushakova OY, Campbell-Thompson M, Deshane JS, Joseph R, Cruz PE, Hauswirth WW, Madsen KM, Croker BP, Berns KI, Atkinson MA, Flotte TR, Tisher CC, Agarwal A. Interleukin 10 attenuates neointimal proliferation and inflammation in aortic allografts by a heme oxygenase-dependent pathway. *Proc Natl Acad Sci U S A.* 2005;102:7251–7256.
9. Mu W, Ouyang X, Agarwal A, Zhang L, Long DA, Cruz PE, Roncal CA, Glushakova OY, Chiodo VA, Atkinson MA, Hauswirth WW, Flotte TR, Rodriguez-Iturbe B, Johnson RJ. IL-10 suppresses chemokines, inflammation, and fibrosis in a model of chronic renal disease. *J Am Soc Nephrol.* 2005;16:3651–3660.
10. Matsushita T, Elliger S, Elliger C, Podsakoff G, Villarreal L, Kurtzman GJ, Iwaki Y, Colosi P. Adeno-associated virus vectors can be efficiently produced without helper virus. *Gene Ther.* 1998;5:938–945.
11. Okada T, Nomoto T, Yoshioka T, Nonaka-Sarukawa M, Ito T, Ogura T, Iwata-Okada M, Uchibori R, Shimazaki K, Mizukami H, Kume A, Ozawa K. Large-scale production of recombinant viruses by use of a large culture vessel with active gassing. *Hum Gene Ther.* 2005;16:1212–1218.
12. Okada T, Nomoto T, Shimazaki K, Lijun W, Lu Y, Matsushita T, Mizukami H, Urabe M, Hanazono Y, Kume A, Muramatsu S, Nakano I, Ozawa K. Adeno-associated virus vectors for gene transfer to the brain. *Methods.* 2002;28:237–247.
13. Kay JM, Keane PM, Suyama KL, Gauthier D. Angiotensin converting enzyme activity and evolution of pulmonary vascular disease in rats with monocrotaline pulmonary hypertension. *Thorax.* 1982;37:88–96.
14. Christman BW, McPherson CD, Newman JH, King GA, Bernard GR, Groves BM, Loyd JE. An imbalance between the excretion of thromboxane and prostacyclin metabolites in pulmonary hypertension. *N Engl J Med.* 1992;327:70–75.
15. Tuder RM, Cool CD, Geraci MW, Wang J, Abman SH, Wright L, Badesch D, Voelkel NF. Prostacyclin synthase expression is decreased in lungs from patients with severe pulmonary hypertension. *Am J Respir Crit Care Med.* 1999;159:1925–1932.
16. Miyata A, Hara S, Yokoyama C, Inoue H, Ullrich V, Tanabe T. Molecular cloning and expression of human prostacyclin synthase. *Biochem Biophys Res Commun.* 1994;200:1728–1734.
17. High K. AAV-mediated gene transfer for hemophilia. *Genet Med.* 2002; 4:56S–61S.
18. Phillips PG, Long L, Wilkins MR, Morrell NW. cAMP phosphodiesterase inhibitors potentiate effects of prostacyclin analogs in hypoxic pulmonary vascular remodeling. *Am J Physiol Lung Cell Mol Physiol.* 2005;288: L103–L115.
19. Ali FY, Egan K, FitzGerald GA, Desvergne B, Wahli W, Bishop-Bailey D, Warner TD, Mitchell JA. Role of prostacyclin versus peroxisome proliferator-activated receptor beta receptors in prostacyclin sensing by lung fibroblasts. *Am J Respir Cell Mol Biol.* 2006;34:242–246.
20. Ameshima S, Golpon H, Cool CD, Chan D, Vandivier RW, Gardai SJ, Wick M, Nemenoff RA, Geraci MW, Voelkel NF. Peroxisome proliferator-activated receptor gamma (PPARgamma) expression is decreased in pulmonary hypertension and affects endothelial cell growth. *Circ Res.* 2003;92:1162–1169.
21. Sitbon O, Humbert M, Nunes H, Parent F, Garcia G, Herve P, Rainisio M, Simonneau G. Long-term intravenous epoprostenol infusion in primary pulmonary hypertension: prognostic factors and survival. *J Am Coll Cardiol.* 2002;40:780–788.
22. Nathwani AC, Gray JT, McIntosh J, Ng CY, Zhou J, Spence Y, Cochrane M, Gray E, Tuddenham EG, Davidoff AM. Safe and efficient transduction of the liver after peripheral vein infusion of self-complementary AAV vector results in stable therapeutic expression of human FIX in nonhuman primates. *Blood.* 2007;109:1414–1421.

Interleukin-10 Expression Mediated by an Adeno-Associated Virus Vector Prevents Monocrotaline-Induced Pulmonary Arterial Hypertension in Rats

Takayuki Ito, Takashi Okada, Hiroshi Miyashita, Tatsuya Nomoto, Mutsuko Nonaka-Sarukawa, Ryosuke Uchibori, Yoshikazu Maeda, Masashi Urabe, Hiroaki Mizukami, Akihiro Kume, Masafumi Takahashi, Uichi Ikeda, Kazuyuki Shimada, Keiya Ozawa

Abstract—Pulmonary arterial hypertension (PAH) is a fatal disease associated with inflammation and pathological remodeling of the pulmonary artery (PA). Interleukin (IL)-10 is a pleiotropic antiinflammatory cytokine with vasculoprotective properties. Here, we report the preventive effects of IL-10 on monocrotaline-induced PAH. Three-week-old Wistar rats were intramuscularly injected with an adeno-associated virus serotype 1 vector expressing IL-10, followed by monocrotaline injection at 7 weeks old. IL-10 transduction significantly improved survival rates of the PAH rats 8 weeks after monocrotaline administration compared with control gene transduction (75% versus 0%, $P<0.01$). IL-10 also significantly reduced mean PA pressure (22.8 ± 1.5 versus 29.7 ± 2.8 mm Hg, $P<0.05$), a weight ratio of right ventricle to left ventricle plus septum (0.35 ± 0.04 versus 0.42 ± 0.05, $P<0.05$), and percent medial thickness of the PA ($12.9\pm0.3\%$ versus $21.4\pm0.4\%$, $P<0.01$) compared with controls. IL-10 significantly reduced macrophage infiltration and vascular cell proliferation in the remodeled PA in vivo. It also significantly decreased the lung levels of transforming growth factor-β_1 and IL-6, which are indicative of PA remodeling. In addition, IL-10 increased the lung level of heme oxygenase-1, which strongly prevents PA remodeling. In vitro analysis revealed that IL-10 significantly inhibited excessive proliferation of cultured human PA smooth muscle cells treated with transforming growth factor-β_1 or the heme oxygenase inhibitor tin protoporphyrin IX. Thus, IL-10 prevented the development of monocrotaline-induced PAH, and these results provide new insights into the molecular mechanisms of human PAH. (*Circ Res.* 2007;101:734-741.)

Key Words: pulmonary hypertension ∎ interleukins ∎ gene therapy ∎ inflammation ∎ vascular smooth muscle cell proliferation

Pulmonary arterial hypertension (PAH) is an intractable disease that leads to increased pulmonary arterial pressure, progressive right heart failure, and premature death; however, no satisfactory treatment for PAH has been established.[1] The pathological process of PAH is characterized by abnormal remodeling of the pulmonary artery (PA) associated with excessive proliferation of pulmonary arterial smooth muscle cells (PASMCs).[2] Accumulating evidence suggests important roles of vascular inflammation in its pathogenesis.[2,3] For instance, serum levels of proinflammatory cytokines such as interleukin (IL)-1 and IL-6 reflect the disease activity in patients with idiopathic PAH.[4] Furthermore, injection of IL-6 can produce PAH and PA remodeling in rats.[5] The remodeled PA presents macrophage infiltration and increased expression of a variety of cytokines, including IL-6, tumor necrosis factor (TNF)-α, and transforming

growth factor (TGF)-β_1.[6,7] Administration of steroids or immunosuppressive drugs decreases the level of PA pressure in patients with PAH.[8,9] These observations suggest a therapeutic potential of targeting inflammation to prevent PAH progression.[10] However, the precise mechanisms underlying the antiinflammatory effects on PA remodeling have not yet been fully investigated.

IL-10 is a multifunctional antiinflammatory cytokine with a vasculoprotective property. During the course of inflammation, IL-10 is produced by type-2 helper T (Th2) lymphocytes, and it inhibits the production of various proinflammatory cytokines in macrophages and Th1 lymphocytes.[11] Exogenous IL-10 prevents proliferative vasculopathy in vivo by inhibiting inflammatory cell infiltration,[12] smooth muscle cell proliferation,[12,13] and chemokine expression.[14] However, clinical efficacy of systemic recombinant IL-10 administra-

Circulation Research is available at http://circres.ahajournals.org

DOI: 10.1161/CIRCRESAHA.107.153023

tion are insufficient because of the lower local IL-10 levels resulting from its short bioactive half-life.[15] In this study, we used an adeno-associated virus (AAV) vector for IL-10 expression because it is an efficient vehicle for systemic and sustained expression of therapeutic proteins.[14] It also has an advantage over other viral vectors in the therapeutic or mechanistic analysis because it produces minimal inflammatory and immune responses in vivo.

Recently, heme oxygenase (HO)-1, an inducible form of HO that promotes production of a vasodilator carbon monoxide (CO), was shown to mediate antiinflammatory and antiproliferative effects of IL-10 in a model of chronic vasculopathy.[12] Increased HO-1 and CO levels attenuated PAH and PA remodeling by inhibiting PASMC proliferation.[16–18] However, no study has explored a direct link between IL-10 and HO-1 in the pathogenesis of PAH. Thus, we examined the effects of IL-10, delivered via an AAV vector, on PA remodeling in a widely-used rat model of PAH induced by the pyrolizidine alkaloid monocrotaline (MCT). We also investigated the mechanisms underlying the effects of IL-10 on the following factors involved in the inflammatory and proliferative vascular changes in PAH: PASMC, macrophage, TGF-β_1, IL-6, and HO-1.

Materials and Methods

AAV Vector Production

DNA encoding rat IL-10 was polymerase chain reaction-amplified from rat splenocyte complementary DNA, using the primers 5'-GCACGAGAGCCACAACGCA-3' and 5'-GATTTGAGTACG-ATCCATTTATTCAAAACGAGGAT-3'. For efficient transgene expression in the skeletal muscle, we constructed a recombinant AAV vector which carried the IL-10 gene (AAV-IL-10) or enhanced green fluorescent protein (eGFP) gene (AAV-eGFP), controlled by the modified chicken β-actin promoter with the cytomegalo virus-immediate early enhancer and the woodchuck hepatitis virus post-transcriptional regulatory element (a kind gift from Dr Thomas Hope, Infectious Disease Laboratory, Salk Institute). AAV vectors were prepared according to the previously described 3-plasmid transfection adenovirus-free protocol with minor modifications to use the active gassing system.[19,20] In brief, 60% confluent human embryonic kidney 293 cells incubated in a large culture vessel with active air circulation were cotransfected with the proviral transgene plasmid, AAV-1 chimeric helper plasmid (p1RepCap), and adenoviral helper plasmid pAdeno (Avigen Inc). The crude viral lysate was purified by 2 rounds of cesium chloride 2-tier centrifugation.[21] The viral stock titer was determined against plasmid standards by dot blot hybridization, after which the stock was dissolved in HN buffer (50 mmol/L HEPES, pH 7.4, 0.15 mol/L NaCl) before injection.

Animal Models

All animal experiments were approved by the Jichi Medical University ethics committee and were performed in accordance with the *National Institute of Health Guide for the Care and Use of Laboratory Animals*. To evaluate the efficiency of in vivo gene expression, 3-week-old male Wistar rats (Clea Japan Inc, Tokyo, Japan) weighing 45 to 55 g were injected with AAV-IL-10 (200 μL, 3×10^{10} to 1×10^{11} genome copies [g.c.] per body) into the bilateral anterior tibial muscles (n=3 animals per group). For hemodynamic and histological analysis, we randomly formed 4 groups comprising 5 rats each: sham rats that were administered the HN buffer (1, NC group); MCT-treated rats administered the HN buffer (2, MCT group); MCT rats administered AAV-eGFP (3, MCT+eGFP group); and MCT rats administered AAV-IL-10 (4, MCT+IL-10 group). After anesthetized with a spontaneous inhalation of 1% isoflurane, the rats in the groups 3 and 4 received intramuscular injection of AAV-eGFP or

AAV-IL-10 (200 μL, 6×10^{10} g.c. per body), respectively. Rats in groups 1 and 2 were injected with the HN buffer (200 μL). MCT (Wako Pure Chemicals) was dissolved in 0.1N HCl, and the pH adjusted to 7.4 with 1.0N NaOH. For hemodynamic and histological studies, all rats except those in the NC group were subcutaneously injected with MCT (30 mg/kg) under the spontaneous inhalation of 1% isoflurane at 4 weeks after vector treatment. For the survival study, rats (n=8 animals/group) were injected with a lethal dose of MCT (45 mg/kg) under the spontaneous inhalation of 1% isoflurane at 4 weeks after vector injection. Survival was estimated from the date of MCT injection until death or 8 weeks after injection.

Hemodynamic Analysis

Four weeks after MCT injection, the rats were anesthetized with spontaneous inhalation of 1% isoflurane, and a tracheotomy was performed. Then, they were mechanically ventilated using a respirator (SAR-830/AP, CWE; tidal volume: 10 mL/kg, respiratory rate: 30 breaths per min) and anesthetized with 0.5% isoflurane through a tracheostomy. After the thoracic cavity was opened using a midsternal approach, 2.0F high-fidelity manometer-tipped catheters (SPC-320, Millar Instruments Inc) were inserted directly into the right or left ventricle. The mean pulmonary arterial pressure (mPAP) or mean aortic arterial pressure (mAoP) was measured using the catheters that were advanced from the right or left ventricle, respectively. The heart rate (HR) was measured by unipolar lead electrocardiography.

Ventricular Weight Measurement and Morphometric Analysis of the PA

After hemodynamic analysis, the rats were euthanized using an overdose isoflurane (5%). The lungs and PAs were perfused with 5 mL of saline followed by 10 mL of cold 4% paraformaldehyde. Each ventricle and the lungs were excised, dissected free, and weighed. The weight ratio of right ventricle to the left ventricle plus septum [RV/(LV+S)] was calculated as an index of right ventricular hypertrophy (RVH). The tissues were fixed in 4% paraformaldehyde for 4 hours, transferred to 30% sucrose in 0.1 mol/L phosphate buffer (pH 7.4) for cryoprotection, and stored at 4°C overnight. Lung tissue was frozen in Tissue-Tek OCT compound (Sakura Finetechnical Co) at −20°C. Then, 7-μm sections were cut using a cryostat. Hematoxylin and eosin (HE) staining was performed on sections from the middle lobe of the right lung, and these were examined using light microscopy. Morphometric analysis was performed in PAs with an external diameter of 25 to 50 and 51 to 100 μm. The medial wall thickness was calculated with the following formula: medial thickness (%)=medial wall thickness/external diameter×100.[22] For quantitative analysis, 30 vessels from each rat were counted and the average was calculated.

Immunohistochemistry

Immunohistochemical staining was performed with monoclonal antibodies against ED1 (1:100; Serotec) and proliferating cell nuclear antigen (PCNA, 1:200; Zymed), using the streptavidin-biotin-peroxidase method, as described previously.[23] ED1 recognizes the lysosomal membrane antigen expressed by a majority of tissue macrophages. Irrelevant mouse immunoglobulin G (Vector Laboratories) was used as a negative control. Reactions were visualized using Vector SG (Vector Laboratories) or 3,3'-diaminobenzidine (Zymed) and counterstained with nuclear fast red or hematoxylin. The number of ED1-positive cells was counted in 250×250-μm fields under 400× magnification and expressed as cells per mm². The number of PCNA-positive cells was quantitatively evaluated as a percentage of total vascular cells in the fields under 1000× magnification. For each rat, the average number or percentage of each cell in 15 randomly selected fields was used for statistical analysis.

Protein Assay

Protein samples were prepared by homogenization of the frozen lung tissue in lysis buffer [10 μmol/L Tris/Cl (pH 8.0), 0.2% NP-40,

1 μmol/L EDTA (pH 7.6)] supplemented with protease inhibitor cocktail Complete Mini (Roche Diagnostics). After centrifugation of the homogenates (3000g for 10 minutes), the supernatants or serum samples were used for measurement. To activate latent TGF-β_1 to an immunoreactive form, the samples were treated with acid according to the manufacturer's instructions (R&D Systems Inc). IL-10 or IL-6 concentrations in the sera and TGF-β_1, IL-6, HO-1, or TNF-α in the lung extracts were measured using enzyme-linked immunosorbent assay (ELISA) kits (Amersham Pharmacia Biotech; R&D Systems). The minimum detectable dose was 3, 3, 16, and 5 pg/mL or 0.78 ng/mL for IL-10, TGF-β_1, IL-6, and TNF-α, or HO-1, respectively. Inter- and intraassay precision of these kits was <10%. The total protein concentrations in the lung extracts were estimated using a BCA Protein Assay kit (PIERCE). The levels of TGF-β_1, IL-6, HO-1, or TNF-α in the lung were expressed as pg per mg protein.

Cell Culture and Proliferation Assay

Human PASMCs were obtained from Clonetics Corp and grown in SmGM-2 medium (Clonetics Corp). PASMCs with a passage between 4 and 6 were used in the experiments. Cells (1×10^3 per well) were incubated in 96-well plates with serum-free Dulbecco's modified Eagle's medium and nutrient mixture F12 (DMEM-F12, Invitrogen) in an atmosphere of 5% CO_2 in the air at 37°C. A tetrazolium-based colorimetric proliferation assay (XTT assay; Cell Proliferation Kit II, Roche Diagnostics) was performed 2 days after adding tin protoporphyrin IX (SnPP; Frontier Scientific), human recombinant TGF-β_1, IL-6, or IL-10 (PeproTech Inc). The optical density between 450 and 650 nm were measured to estimate the number of viable cells.

Statistical Analysis

Data from multiple experiments are expressed as mean±SEM. Statistical analysis and correlations were performed using StatView (Abacus Concepts, Inc). Survival curves were analyzed using the Kaplan–Meier method and compared by log-rank tests. Differences in other parameters were evaluated by analysis of variance combined with Fisher test. The correlation test was used to measure the association between 2 variables. A value of $P<0.05$ was considered statistically significant.

Results

AAV Vector-Mediated IL-10 Expression Improves Survival of MCT-PAH Rats

Eight weeks after AAV-IL-10 injection, serum IL-10 concentrations were elevated in a vector dose-dependent manner (Figure 1A). We determined that injection with AAV-IL-10 (6×10^{10} g.c. per rat) significantly increased serum IL-10 levels as compared with untreated controls (184.1±47.6 versus 18.8±1.3 pg/mL, $P<0.05$, n=3 each). In contrast, injection with MCT (Figure 1A) or AAV-eGFP alone (data not shown) caused no significant change in serum IL-10 levels. Therefore, we used this dosage for all vectors in subsequent experiments. For survival analysis, the rats were injected with a lethal dose of MCT, after 4 weeks of vector injection. The survival in IL-10–transduced rats was significantly improved as compared with the eGFP-transduced rats 8 weeks after MCT injection (75% versus 0%, $P<0.01$, n=8 each; Figure 1B).

Effects of IL-10 on PAH and RVH

Four weeks after MCT injection, the mPAP levels were significantly higher than those of the untreated controls (30.1±4.0 versus 20.0±2.1 mm Hg, $P<0.01$, n=5 each; Figure 2A). Treatment with AAV-IL-10 but not AAV-eGFP significantly inhibited the elevation of mPAP (22.8±1.5
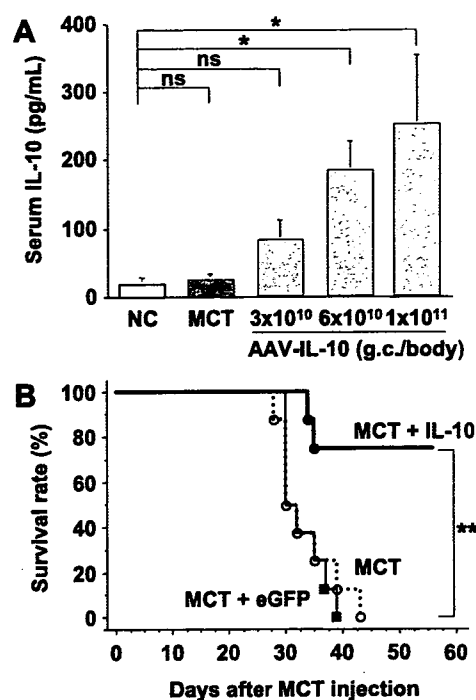

Figure 1. Adeno-associated virus (AAV) vector-mediated systemic interleukin (IL)-10 expression improves survival of monocrotaline (MCT)-induced pulmonary arterial hypertension (PAH) rats. A, In vivo IL-10 expression induced by AAV-IL-10. Serum IL-10 concentrations (pg/mL) were determined using ELISA 8 weeks after a single intramuscular injection of AAV-IL-10 into the anterior tibial muscles of 3-week-old Wistar rats. Genome copies (g.c.) per rat were as indicated. Data represent mean±SEM (n=3 animals per group, *$P<0.05$). ns indicates not statistically significant; NC, untreated controls. B, The Kaplan-Meier survival curve in MCT-PAH rats. The Wistar rats were treated with a lethal dose of MCT 4 weeks after the single intramuscular injection of HN buffer (MCT group), AAV-eGFP (MCT+eGFP group), or AAV-IL-10 (MCT+IL-10 group). n=8 animals per group, **$P<0.01$ versus MCT or MCT+eGFP groups.

versus 29.7±2.8 mm Hg, $P<0.01$, n=5 each; Figure 2A). Moreover, serum IL-10 concentrations correlated negatively with mPAP in MCT-treated rats ($r=-0.75$, $P<0.01$, n=15; Figure 2B). In contrast, this IL-10 expression caused no significant change in HR (data not shown) and mAoP (76.7±2.1 versus 74.6±6.8 mm Hg, MCT+IL-10 versus MCT+eGFP group, n=5 each). IL-10 expression also has a beneficial effect on RVH. Four-week MCT treatment significantly increased the RV/(LV+S) values as compared with the untreated controls ($P<0.01$, n=5 each; Figure 2C). Treatment with AAV-IL-10 but not AAV-eGFP inhibited MCT-induced increase of RV/(LV+S) significantly ($P<0.05$, n=5 each; Figure 2C). Furthermore, serum IL-10 concentrations correlated negatively with RV/(LV+S) in MCT-treated rats ($r=-0.57$, $P<0.05$, n=15; Figure 2D). These results indicate that sustained IL-10 expression prevented the development of MCT-induced PAH and RVH.

Effects of IL-10 on Histological Changes of the PA

Medial hypertrophy is a hallmark of pathological vascular remodeling in PAH. Four weeks after MCT injection, the medial thickness of PAs was markedly increased in the MCT-treated rats compared with untreated controls ($P<0.01$,
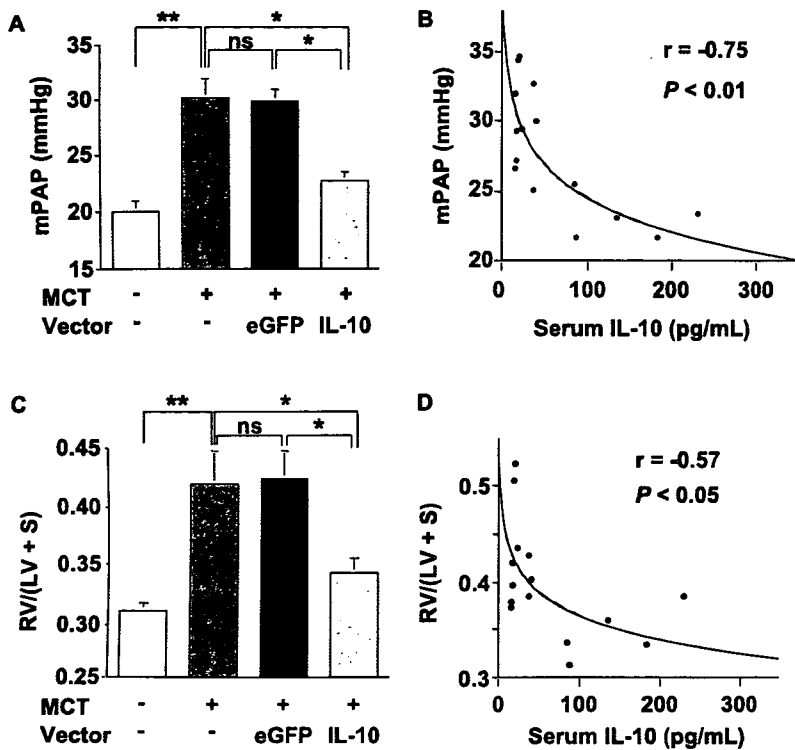
Figure 2. Effects of IL-10 on PAH and right ventricular hypertrophy (RVH). The 7-week-old Wistar rats were treated with monocrotaline (MCT) 4 weeks after vector injection. A, Statistical analysis of mean pulmonary arterial pressure (mPAP, mm Hg) determined by direct catheterization 4 weeks after MCT injection. Data represent the mean±SEM (n=5 animals per group; *$P<0.05$, **$P<0.01$). ns indicates not statistically significant. B, Correlation between serum IL-10 concentrations and mPAP levels in the MCT-treated rats (groups: MCT, MCT+ eGFP, or MCT+IL-10; n=5 animals per group; $r=-0.75$, $P<0.01$). C, Quantitative RVH analysis. The weight ratio of the right ventricle to left ventricle plus septum [RV/(LV+S)] is presented as an index of RVH (n=5 animals per group; *$P<0.05$, **$P<0.01$). D, Correlation between serum IL-10 concentrations and RV/(LV+S) in the MCT-treated rats (groups: MCT, MCT+ eGFP, and MCT+IL-10; n=5 animals per group; $r=-0.57$, $P<0.05$).

n=5 each; Figure 3B, 25 to 50 μm; Figure 3C, 51 to 100 μm in external diameter). Treatment with AAV-IL-10 but not AAV-eGFP significantly inhibited the increase in percent medial thickness ($P<0.01$, n=5 each). Inflammatory cell infiltration and vascular cell proliferation are also important indicators in the progression of PA remodeling. Immunohistochemical analysis shows that treatment with AAV-IL-10 significantly decreased the number of accumulated macrophages (ED1-positive cells; $P<0.01$, n=5 each; Figure 3D) and proliferating vascular cells (PCNA-positive cells; $P<0.01$, n=5 each; Figure 3E) in the PA of MCT-treated rats as compared with treatment with MCT alone or AAV-eGFP.

Effects of IL-10 on Cytokine Expression

We analyzed pulmonary tissue and serum cytokine levels relevant to the pathogenesis of PAH. Four weeks after MCT injection, the TGF-β_1 and IL-6 levels in the MCT-treated rats were significantly higher than those of the untreated controls ($P<0.01$, n=5 each; Figure 4A and 4C). Treatment with AAV-IL-10 but not AAV-eGFP significantly inhibited the MCT-induced elevation of TGF-β1 and IL-6 levels ($P<0.01$, n=5 each). Furthermore, these levels correlated positively with the percent medial thickness in the rats with or without MCT treatment ($r=0.84$, $P<0.01$; $r=0.87$, $P<0.01$, respectively; Figure 4B and 4D).

HO-1 has been reported to mediate the antiinflammatory effects of IL-10.[24] Treatment with AAV-IL-10 but not AAV-eGFP or MCT alone significantly increased the lung HO-1 levels as compared with untreated controls ($P<0.05$, n=5 each, Figure 4E). In addition, HO-1 levels correlated negatively with IL-6 levels in MCT-treated rats ($r=-0.85$, $P<0.01$; Figure 4F). In contrast, serum IL-6 levels positively correlated with lung IL-6 levels ($r=-0.69$, $P<0.01$; Figure

4G). Although the lung TNF-α levels significantly increased in MCT-treated rats compared with untreated controls, IL-10 expression caused no change in the lung TNF-α levels (Figure 4H).

Effects of IL-10 on PASMC Proliferation

To determine whether IL-10 directly inhibits PASMC proliferation, we performed an in vitro colorimetric XTT assay using cultured human PASMCs. Treatment of PASMCs with SnPP, which inactivates HO-1, and treatment with TGF-β_1 or IL-6 dose dependently promoted cell proliferation (n=4 each, $P<0.05$; Figure 5A through 5C). Treatment with IL-10 alone had no significant effect on PASMC proliferation (Figure 5D). On the other hand, pretreatment with IL-10 significantly inhibited PASMC proliferation induced by SnPP or TGF-β_1 (n=4 each, $P<0.05$; Figure 5E) but not that induced by IL-6.

Discussion

The present study demonstrates that IL-10, delivered by an intramuscular injection of an AAV1 vector, prevented the development of MCT-PAH in rats. Systemic IL-10 expression also improved survival in rats and prevented the development of RVH and medial hypertrophy of PA. IL-10 also reduced macrophage accumulation, vascular cell proliferation, and pulmonary tissue levels of TGF-β_1 and IL-6, all of which play pivotal roles in progression of PA remodeling. Further, IL-10 enhanced HO-1 levels in the lung. Thus, IL-10 exerts multiple preventive effects on inflammatory and proliferative PA remodeling (Figure 6).

Blockade of a single proinflammatory signaling pathway by IL-1 or monocyte chemoattractant protein-1 attenuates PA remodeling.[25,26] However, the prosurvival effects of antiinflammatory molecules on PAH animals have not been re-
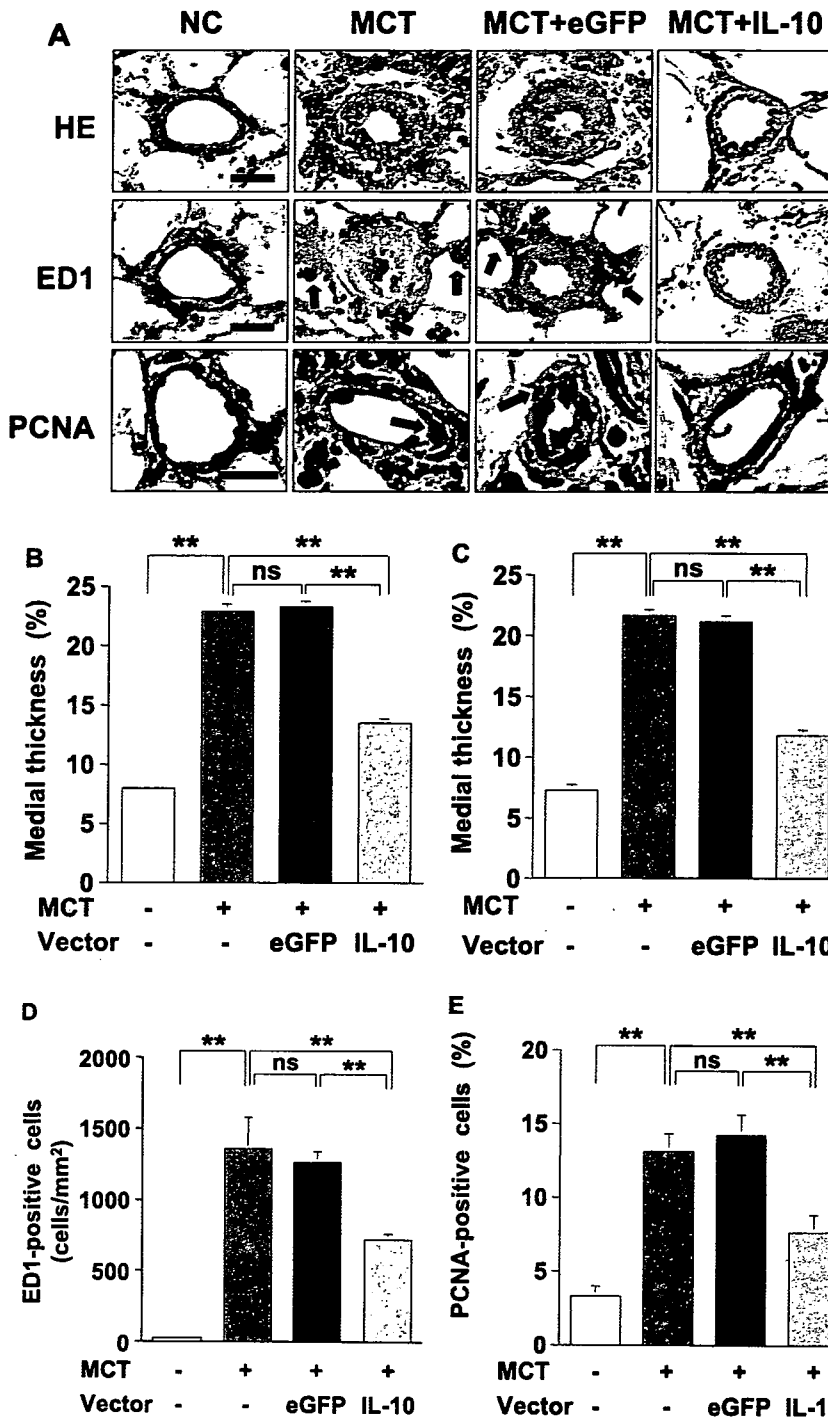
Figure 3. Antiinflammatory and antiproliferative effects of IL-10 on the remodeled pulmonary artery (PA). The 7-week-old Wistar rats were treated with MCT 4 weeks after vector injection. Representative cross-sectional views of the peripheral PAs stained with HE or immunohistochemistry (ED1 or PCNA) 4 weeks after MCT treatment (A; original magnification ×1000, Scale bar=20 μm). Blue arrows indicate ED-1-positive cells and red arrows, PCNA-positive cells. Quantification of percent medial thickness for vessels 25 to 50 μm (B) and 51 to 100 μm (C) in external diameter. Quantitative analysis of the number of perivascular macrophages (ED-1-positive cells, D) and proliferating vascular cells (PCNA-positive cells, E). Data represent mean±SEM (n=5 animals per group, **$P<0.01$). ns indicates not statistically significant.

ported. Evidence of right heart failure is involved in the mortality of MCT-PAH rats. In this study, all rats treated with a lethal dose of MCT exhibited symptoms of right heart failure such as pleural effusion and body weight decrease. In the setting of severe PAH and right heart failure, cytokine networks may orchestrate disease progression. Thus, blockades of multiple inflammatory signals might be responsible for the prosurvival effect of IL-10.

IL-10 has gained significant attention because of its suppressive influence on inflammatory and proliferative vasculopathy. The IL-10 receptor is expressed on vascular smooth muscle cells (VSMCs). IL-10 inhibits inflammation and VSMC proliferation in arterial remodeling after balloon injury or transplant rejection.[12,13] Consistent with previous studies using MCT-PAH,[6,7] we demonstrate that increased levels of TGF-β_1 and IL-6 are related to PASMC proliferation and PA remodeling progression. Although treatment with IL-10 alone caused no significant effects on PASMC proliferation,[27] IL-10 significantly inhibited the lung TGF-β_1 expression and TGF-β_1-induced PASMC proliferation. TGF-β_1 enhances PASMC proliferation of idiopathic PAH patients but not that of normal subjects or secondary PAH patients.[28]
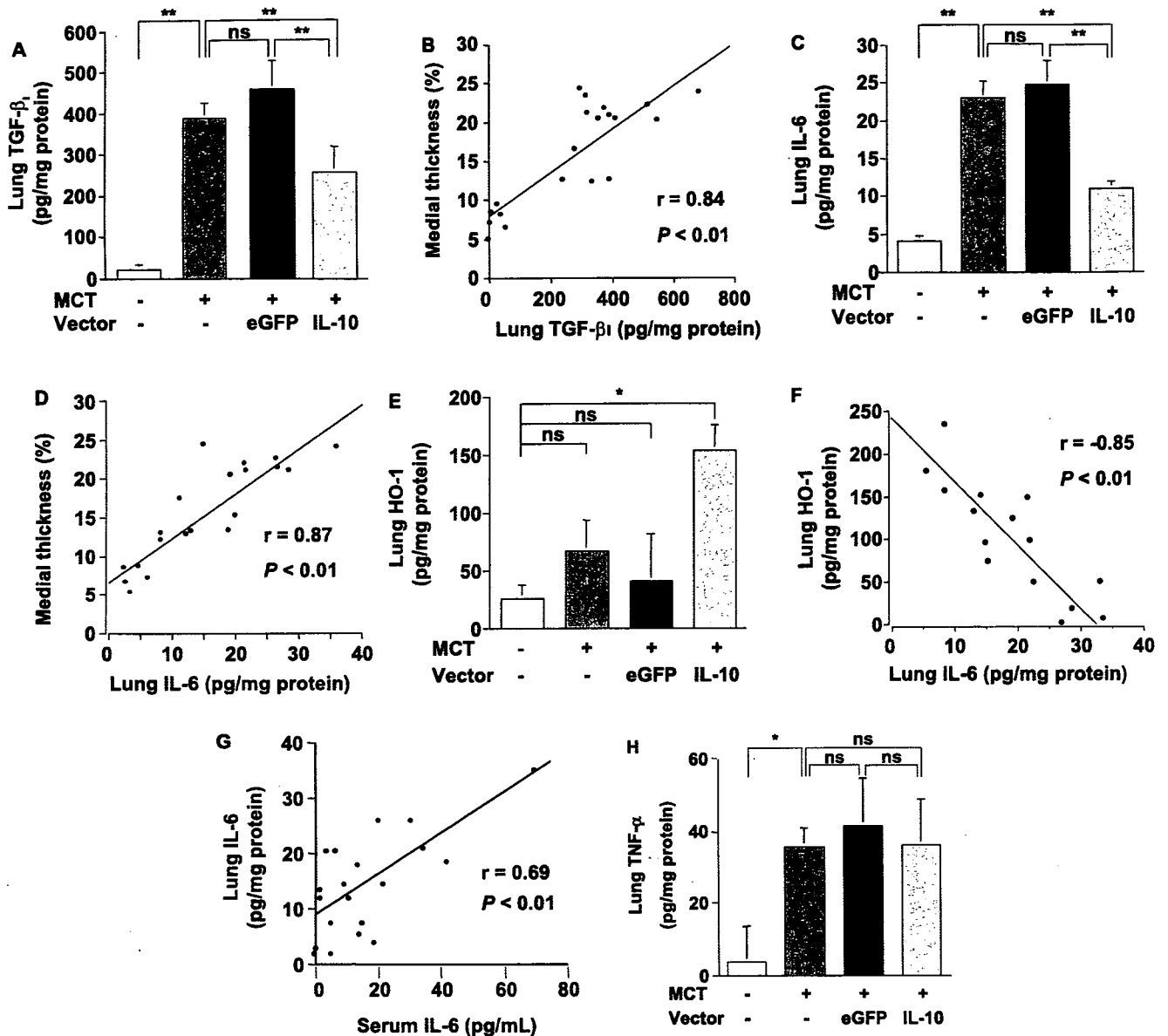
Figure 4. Effects of IL-10 on expression of transforming growth factor-β_1 (TGF-β_1), IL-6, heme oxygenase-1 (HO-1), and tumor necrosis factor-α (TNF-α) in the lung. The 7-week-old Wistar rats were treated with MCT 4 weeks after vector injection. Concentrations of active TGF-β_1 (A), IL-6 (C), HO-1 (E), and TNF-α (H) in the lung extracts were detected using ELISA 4 weeks after MCT treatment. Data represent mean±SEM (n=5 animals per group; *P<0.05, **P<0.01). ns indicates not statistically significant. Correlation between the percent medial thickness and lung levels of TGF-β_1 (B) or IL-6 (D) in rats (groups: NC, MCT, MCT+eGFP, or MCT+IL-10; n=5 animals per group; r=0.84, P<0.01 and r=0.87, P<0.01, respectively). Correlation between the HO-1 and IL-6 (F) levels in the rat lung (groups: MCT, MCT+eGFP, or MCT+IL-10; n=5 animals per group; r=-0.85, P<0.01). Correlation between the lung and serum IL-6 levels (G) in rats (groups: NC, MCT, MCT+eGFP, or MCT+IL-10; n=5 animals per group; r=0.69, P<0.01).

Additionally, TGF-β_1 is accumulated in the hypertrophic PA of both human PAH and MCT-PAH[29,30] and exacerbates PA remodeling.[31]

IL-6, a multifunctional proinflammatory cytokine, acts as a strong mitogen to promote VSMC proliferation.[11] Macrophage infiltration is a hallmark of PAH progression, and activated macrophages produce substantial amounts of IL-6 in MCT-PAH rats.[6,32] In this study, IL-10 treatment inhibited perivascular macrophage infiltration and the lung IL-6 expression in vivo but not IL-6-induced PASMC proliferation in vitro. These results suggest that IL-10 may attenuate IL-6 function indirectly through the decreased accumulation of perivascular macro-

phages and IL-6. Furthermore, the serum IL-6 levels significantly correlated with the lung IL-6 levels. Because serum IL-6 level reflects the disease activity of idiopathic PAH, it can be a useful biomarker of antiinflammation therapy of PAH. On the other hand, IL-10 did not affect the MCT-induced TNF-α expression in the lung. However, previous studies demonstrated that IL-10 prevents TNF-α-induced VSMC proliferation in vitro.[27] These observations suggest that IL-10 might modulate the downstream signal of TNF-α but not its expression in the setting of MCT-PAH. Overall, IL-10 affects the dynamics of cytokine networks involved in PA remodeling, and its site of action may differ according to the cytokine signal.